Arabian Journal of Geosciences (2021) 14: 811
https://doi.org/10.1007/s12517-021-07009-2

ORIGINAL PAPER

Mapping soil erosion–prone sites through GIS and remote sensing for the Tifnout Askaoun watershed, southern Morocco

Abdellaali Tairi[1] · Ahmed Elmouden[1] · Lhoussaine Bouchaou[1,2] · Mohamed Aboulouafa[3]

Received: 11 July 2019 / Accepted: 22 March 2021 / Published online: 3 May 2021

Abstract

The Moroccan High Atlas is very sensitive to soil erosion due to its steep slopes, torrential rains, and degraded plant cover. The degradation of fertile soils in this mountainous watershed influences negatively upon agricultural productivity. The objective of this study is to quantify soil erosion in the Tifnout Askaoun watershed in southern Morocco. The Revised Universal Soil Loss Equation (RUSLE), the geographic information system (GIS) techniques, and the Tropical Rainfall Measuring Mission (TRMM) data were adopted for mapping the annual rate of soil loss in this watershed area of around 1488 km^2. The spatial distribution of annual soil erosion rates was obtained by integrating the geo-environmental variables into a GIS. These variables are the rainfall erosivity (*R*) generated from the TRMM data, the soil erodibility factor (*K*), the length and slope inclination (LS), the vegetation and management factor (*C*), and the practice support factor (*P*). Results reveal an average annual soil erosion rate of 14.44 t/ha/year and a good correlation with the slope length and steepness factor ($r = 0.72$) and in a lesser extent with the rainfall erosivity factor ($r = 0.63$). The sub-catchments of the study area were mapped and grouped into five classes of vulnerability to soil erosion risk, with results indicating that the Toubkal sub-catchment is the most threatened by water erosion risk as reflected by an average erosion rate of 48.05 t/ha/year. Approaches and results from this study, which was conducted between 2017 and 2019, may benefit researchers and decision-makers concerned with soil management primarily in mountainous areas where soil degradation impacts the activities of the rural population.

Keywords Soil loss · RUSLE · GIS · Tifnout Askaoun · High Atlas Mountains · Morocco

Responsible Editor: Stefan Grab

✉ Abdellaali Tairi
tairiabdel@gmail.com

Ahmed Elmouden
a.elmouden@uiz.ac.ma

Lhoussaine Bouchaou
l.bouchaou@uiz.ac.ma

Mohamed Aboulouafa
mohammed.aboulouafa@uit.ac.ma

1 Laboratory of Applied Geology and Geo-Environment, Department of Geology, Faculty of Science, Ibn Zohr University, Agadir, Morocco

2 International Water Research Institute (IWRI), Mohammed VI Polytechnic University (UM6P), Rabat, Morocco

3 Laboratory of Materials, Electrochemistry and Environment, Department of Chemistry, Faculty of Science, Ibn Tofail University, Kenitra, Morocco

Introduction

Soil is the most important vital natural resource that supports crucial ecosystem functions and provides several crucial environmental resources (Kouli et al. 2009; Alexakis et al. 2013). Soil erosion is a movement of sediments and organic matter from one place to another by a transport agent which is the runoff in the case of water erosion (Ellison 1946; Foucault and Raoult 1995; Enters 1998). It is considered as a major environmental problem since it negatively threatens natural resources and the environment (Rahman et al. 2009). It leads to the loss of essential soil elements, a scarcity of land resources, and endangers the richness of species and the equilibrium of the ecosystems. This causes a decline in global agricultural production and economic development (Pimentel and Burgess 2013). These harmful consequences are both at the level of the source where it could lead to desertification and at the level of the sediment reception areas where it causes siltation of hydraulic structures which would

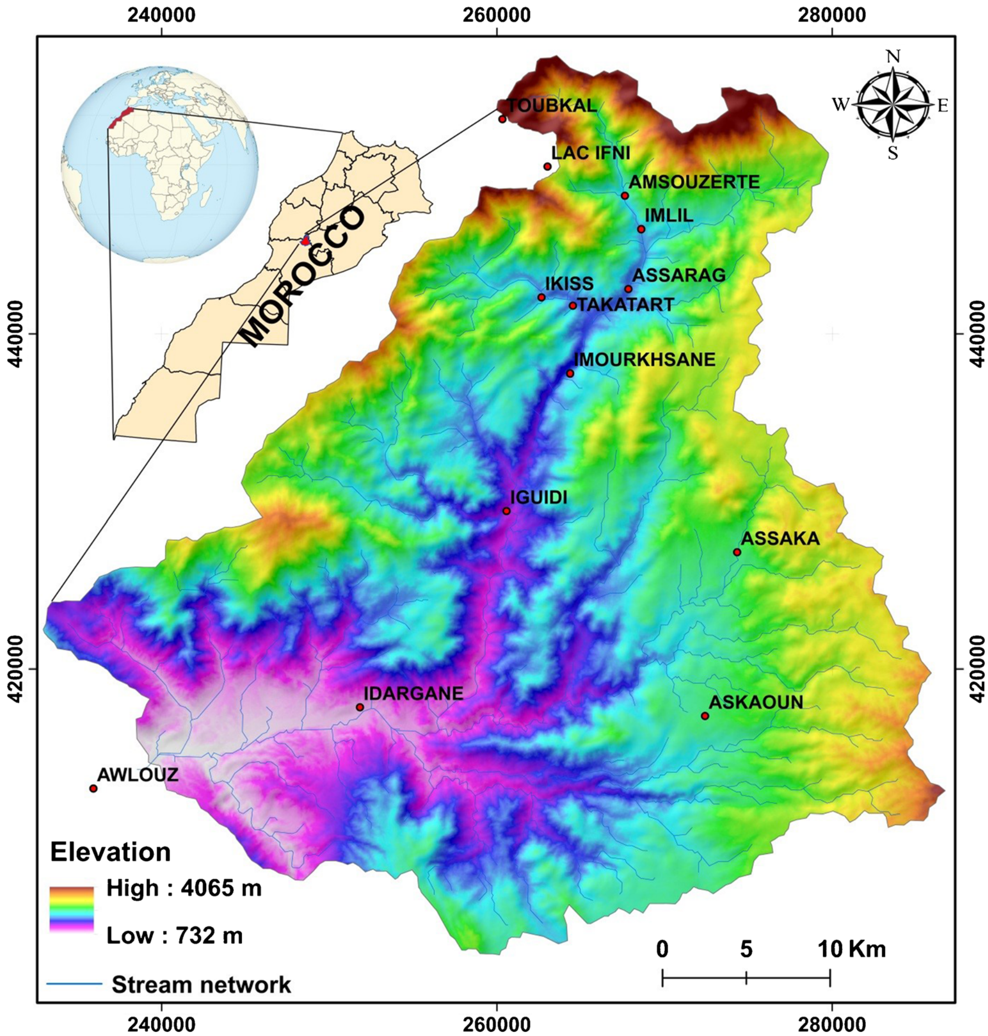

Fig. 1 Geographical location with elevation variation of the study area

lead to flooding (Van Pelt et al. 2017). The consequences of soil degradation range from reduced soil fertility to the evacuation of entire regions (Roy et al. 2005).

This phenomenon is accentuated especially in regions with an arid to semiarid climate. The negative effects of soil erosion on the environment are now a topic of concern to researchers and scientists around the world (Pal and Chakrabortty 2019; Saha et al. 2020), and obviously, the quantitative water erosion mapping has attracted a lot of attention (Tuo et al. 2018; Vaezi et al. 2017). Many methods have been developed for the quantification and calculation of the erosion rate either measured directly in the field or estimated by soil analyses or empirical models and equations that take into account the impact of all variables of soil erosion (Lu et al. 2004; Moukhchane 2002; Prasannakumar et al. 2012; Tian et al. 2009). Among these are the universal soil loss equation (USLE) (Wischmeier and Smith 1978), the European Soil Erosion Model (EUROSEM) (Morgan et al. 1990), the Soil and Water Assessment Tool (SWAT) (Engel et al. 1993), the Mediterranean Desertification and Land Use (MEDALUS) (Kirkby et al. 1998), the Revised Universal Soil Loss Equation (RUSLE) which is an improved version of the USLE model (Renard 1997; Renard et al. 1991), etc. Thanks to the easy access to various input data and its precision, the RUSLE model remains the most widely used tool for soil erosion quantification studies around the world (Khan and Govil 2020; Mahala 2018) and remains a very good evaluation model that can easily be integrated into a GIS environment (Nehaï and Guettouche 2020; Pradeep et al. 2015).

Remote sensing and GIS are particularly powerful tools for the study of natural hazards (Abuzied et al. 2016a, 2016b). They are essential tools in interactive decision support systems for natural hazard management operations (Abuzied and Alrefaee 2019; BouKheir et al. 2006; Shrimali et al. 2001; Wachal and Hudak 2000).

In Morocco, as everywhere in the world, this phenomenon depends on several natural physico-climatic factors (e.g., rainfall, vegetation, lithology, topography, soil erodibility, etc.) and anthropogenic factors (e.g., cultivation on slopes, deforestation, hydraulic and civil engineering).

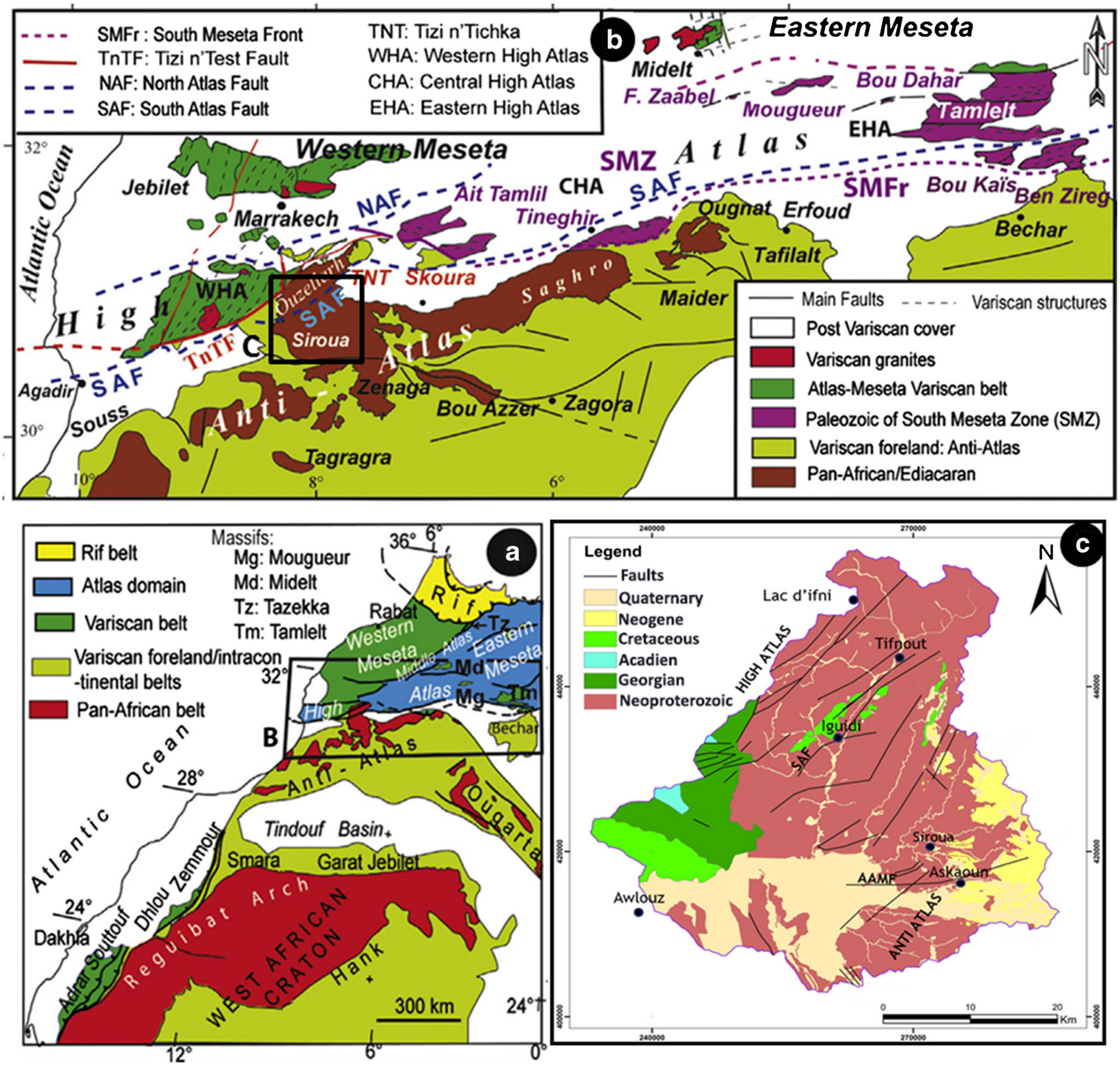

Fig. 2 **a** Simplified geological map of Morocco (Western High Atlas, Meseta domain, and the Anti-Atlas) at the northern margin of the WAC (adapted from Hoepffner et al. 2005; Ouabid et al. 2017; EL Haibi et al. 2020). **b** Zoom of the contact area between the high Atlas and the Anti-Atlas and the location of the study area. **c** Simplified geological map of the Tifnout Askaoun watershed

The Tifnout Askaoun watershed, located in southern Morocco between the high-altitude mountains of the High Atlas and the Anti-Atlas, is exposed highly to erosion because of different aspects (shape, high variable rainfall, rivers discharge, steep slope, and poorly developed soils) (Tairi et al. 2019; Bouchaou et al. 2008). Given this background, the purpose of this study is to map the annual erosion rate in the Tifnout Askaoun watershed, using the Revised Universal Soil Loss Equation in a GIS environment. Results should also allow to highlight the most threatened sub-catchments by the phenomenon of water erosion that requires priority intervention.

Materials and methods

Study area

The “Tifnout Askaoun” zone is located between the latitudes North 30° 35′ and 31° 05′ and the longitudes West 7° 37′and 8° 11′. This zone includes, in the north, the large Tifnout valley, which represents the southern flank of the western High Atlas Mountains, and the south Askaoun zone which represents the Siroua mountain of the Anti-Atlas. This highly mountainous region is mainly drained to the north by the Assif

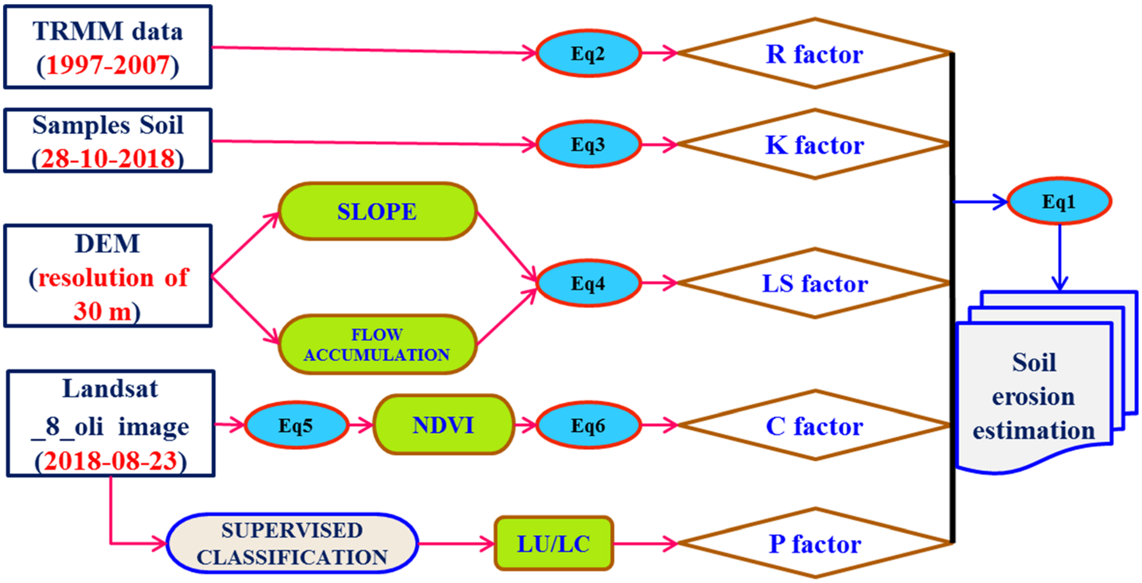

Fig. 3 The methodological framework for implementing the RUSLE model for soil erosion

Tifnout and to the south by the different wadis of Askaoun. It is characterized by very rugged topography with altitudes ranging from 732 m.a.s.l. in the southern part of the Tifnout valley to 4065 m.a.s.l. near the summit of Toubkal (Fig. 1).

Geology

The Tifnout Askaoun watershed includes two main mountain ranges (Fig. 2):

In the east

The Siroua Massif forms the link between the High Atlas and the Anti-Atlas, which explains the confusion often made in its identification with one or the other of these two chains. It is a mountainous area that is difficult to access, with an average altitude of close to 2000 m and with a summit of 3304 m (mountain of Siroua). This was visited at the beginning of the twentieth century (Gentil 1905). It is located in the central zone of the Anti-Atlas and belongs to the Pan-African Neoproterozoic domain. It is made up of a Pan-African basement and Upper to Terminal Neoproterozoic volcanic cover, as well as a much more recent Cretaceous and Neogene cover (Belkacim et al. 2017). This massif is cut to the south by the Anti-Atlas Major Fault (AAMF) (Choubert 1947) (Fig. 2).

In the north

The Moroccan High Atlas is located north of the South Atlas Fault (SAF) which boards, in the south, the Anti-Atlas mountain constituting the northern limit of the West African

Table 1 Characteristics of the used Landsat 8 OLI data

	Bands	Wavelength (micrometers)	Resolution (meters)
Landsat 8 OLI and Thermal Infrared Sensor (TIRS)	Band 1, coastal aerosol	0.43–0.45	30
	Band 2, blue	0.45–0.51	30
	Band 3, green	0.53–0.59	30
	Band 4, red	0.64–0.67	30
	Band 5, near-infrared	0.85–0.88	30
	Band 6, SWIR 1	1.57–1.65	30
	Band 7, SWIR 2	2.11–2.29	30
	Band 8, panchromatic	0.50–0.68	15
	Band 9, circus	1.36–1.38	30
	Band 10, thermal infrared 1	10.60–11.19	100
	Band 11, thermal infrared 2	11.50–12.51	100

Table 2 Thematic evaluation of the land cover map

	Water	Dense forest	Agricultural land	Open forest	Fallow land	Settlement	Barren land	Total user	User accuracy (%)
Water	5	0	0	0	0	0	0	5	100
Dense forest	0	30	3	0	0	0	0	33	90.91
Agricultural land	0	0	42	8	0	0	3	53	79.25
Open forest	0	2	0	47	0	0	10	59	79.66
Fallow land	0	0	0	0	16	0	7	23	69.57
Settlement	0	0	0	0	0	10	2	12	83.33
Barren land	0	0	0	1	2	0	53	56	94.64
Total (producer)	5	32	45	56	18	10	75	241	
Producer accuracy	100	93.75	93.33	83.93	88.89	100	70.67		
Overall map accuracy (%)	84.23								
Kappa	0.80								

Craton (WAC) (Ennih and Liégeois 2001; Taib et al. 2020) (Fig. 2a and b). The High Atlas chain contains the highest peaks in all of North Africa (Toubkal 4167 m), with interior plateaus and basins and deep valleys like the Tifnout valley. The heart of the chain is of Paleozoic age where Georgian and Acadian lands outcrop in the western part of the study area with sandstone and quartzite lithologies (Michard et al. 2010; Missenard 2006). The Quaternary lands are negligible except to the south of the watershed in the form of alluvium at the bottom of the wadis (Fig. 2c).

Datasets

The process of soil degradation that affects our study area results from the interaction of several factors. To conduct this study, we used the following documents:

- Monthly and annual rainfall data taken from the Tropical Rainfall Measuring Mission (TRMM) for a period of 12 years (1998–2009). Date were collected from the NASA database, which can be downloaded free of charge from https://disc.gsfc.nasa.gov/.
- A Landsat 8 OLI satellite image (date_acquisition = 2018-08-23, (path/row 202/35), downloadable for free from the site of US Geological Survey (USGS) http://earthexplorer.usgs.gov/. Interpreted and classified to define land use.
- A digital elevation model (30 m): a product of the Ministry of Economy, Trade and Industry, Japan (METI), and the National Aeronautics and Space Administration (NASA); downloadable for free from www.jspacesystems.or.jp/ersdac/GDEM/E/4.html.
- The results of granulometry analysis and organic carbon of the soils sampled as of October 28, 2018, in the study area.

Pre-processing of the datasets

Before compiling all the factors, the raw datasets were georeferenced with Universal Transverse Mercator (UTM)

Table 3 *P* values assigned for each land cover and land use classes

Land use–/land cover–type *P* values	Land use–/land cover–type *P* values	Reference
Dense forest	1.0	Dai et al. 2013; Xu et al. 2013
Open forest	0.8	Teng et al. 2018
Water	1.0	Dutta et al. 2015; Naqvi et al. 2013
Agricultural land	0.5	Dutta et al. 2015; Naqvi et al. 2013
Settlement	1.0	Dutta et al. 2015; Naqvi et al. 2013
Fallow land	0.9	Sun et al. 2014
Barren land	1.0	Dai et al. 2013; Zhang et al. 2016

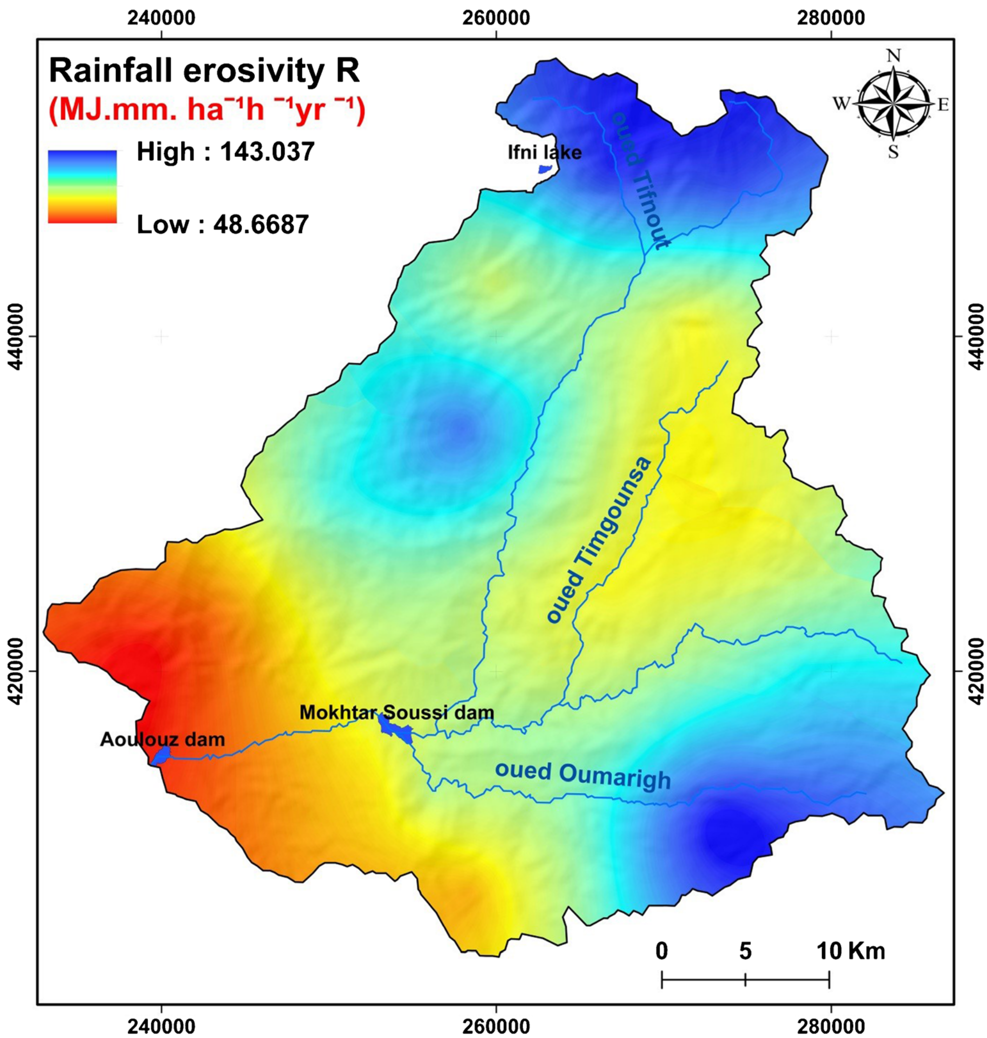

Fig. 4 Rainfall erosivity map (R)

projection using WGS 1984 datum. The boundary of the Tifnout Askaoun watershed was delineated from the DEM using the spatial analyst tool of ArcGIS (10.4.1). And it was used for subsetting the Landsat image, TRMM images, and projection of the soil samples. All the processing of the Landsat image was achieved using ENVI 5.3 software.

Methods

The RUSLE model was used in the GIS platform to map the spatial distribution of the soil loss rate in the Tifnout Askaoun watershed. This model uses five parameters considered as essential water erosion factors related to precipitation, soil characteristics, topography, and land use (Eq. 1 and Fig. 3):

$$A = R*K*LS*C*P \quad (1)$$

where:

A is the annual loss of soil in (tons $ha^{-1}yr^{-1}$).
R is the rainfall erosivity factor in (MJ.mm. $ha^{-1}h^{-1}yr^{-1}$).
K is the soil erodibility factor in (t ha^{-1} h^{-1} ha^{-1} $MJ^{-1}mm^{-1}$).
LS is the topographic factor (dimensionless).
C is the cropping management factors (dimensionless).
P is the practice support factor (dimensionless).

The RUSLE model is one of the best models for quantifying the rate of soil erosion, characterized by ease of use and satisfactory efficiency (Chafai et al. 2020). All the data entered into the geographic information system (GIS) enabled us to obtain the map of the risk of erosion in the Tifnout Askaoun watershed. According to several studies, the RUSLE model gives reliable results at the scale of watersheds all over the world and in particular in the Mediterranean countries (Bonn 1998; Smith 1999).

Generation of RUSLE factors The model (RUSLE) has long been applied to watersheds to estimate annual soil losses. It is an easily applicable model as these input parameters can be

Table 4 Physical properties of soil samples and calculation of Fc sand, Fcl-si, F org C, F hisand, and *K* values (sampling date: October 28, 2018)

Soils	Sand %	Silt %	Clay %	C org carbon %	Fcsand	F cl-si	F orgc	F hisand	*K* value
1	30.11	48.56	18.57	2.06	0.47	0.90	0.9998677	1	0.057
2	46.40	33.57	18.57	1.69	0.46	0.87	0.9998927	1	0.054
3	77.86	7.13	12.86	0.25	0.44	0.73	0.9999848	1	0.043
4	35.09	41.25	22.86	1.94	0.47	0.87	0.9998755	1	0.055
5	56.54	24.89	17.14	1.12	0.45	0.85	0.9999302	1	0.052
6	66.37	16.33	15.71	1.35	0.45	0.81	0.9999151	1	0.049
7	55.54	20.15	22.86	1.12	0.46	0.79	0.9999297	1	0.048
8	44.66	42.31	12.86	1.94	0.46	0.92	0.9998755	1	0.057
9	56.51	35.23	7.14	1.99	0.45	0.94	0.9998724	1	0.057
10	73.40	12.12	12.86	0.80	0.44	0.80	0.9999503	1	0.048
11	71.86	17.12	10.00	2.22	0.44	0.87	0.9998565	1	0.052
12	61.17	24.25	12.86	1.93	0.45	0.88	0.9998764	1	0.053
13	51.74	21.04	25.71	1.07	0.46	0.78	0.9999328	1	0.048
14	67.34	16.33	15.71	1.97	0.45	0.81	0.9998738	1	0.049
15	69.71	17.21	14.29	1.95	0.45	0.83	0.9998747	1	0.050
16	73.38	9.36	15.71	2.14	0.44	0.74	0.999862	1	0.044
17	77.84	4.30	17.14	1.94	0.44	0.61	0.9998755	1	0.036
18	57.30	34.56	7.14	1.60	0.45	0.94	0.9998985	1	0.057
19	49.68	35.21	17.14	2.29	0.46	0.88	0.9998519	1	0.054
20	58.90	24.12	15.71	2.47	0.45	0.86	0.999839	1	0.052
21	57.82	32.11	10.00	2.47	0.45	0.92	0.9998393	1	0.056
22	71.28	10.28	21.14	1.04	0.45	0.71	0.9999353	1	0.042
23	61.60	15.22	22.86	1.91	0.45	0.75	0.9998776	1	0.046
24	60.80	19.21	20.00	1.51	0.45	0.80	0.9999044	1	0.049

generated from the available institutional data. The data used for the elaboration of the different parameters are a satellite image Landsat 8 OLI; a digital elevation model (DEM) of 30-m resolution; monthly and annual rainfall data provided by the TRMM data and results of granulometry analysis, and organic carbon of soil samples collected during the field trip on January 15, 2019, in the study area. We describe below the different factors used in the model.

Rainfall erosivity (R) factor The *R* factor represents the susceptibility of detachment and displacement by the transport of soil particles by raindrops (Teng et al. 2018). The effect of the *R* factor is increased by the intense rains and the accumulation of moderate rains (Wischmeier and Smith 1978). In the absence of the availability of the rainfall data necessary for the calculation of the *R* factor, we used the data provided by the Tropical Rainfall Measuring Mission (TRMM) between 1998 and 2009 provided with open access on the NASA website. This satellite is a joint mission between NASA and the Japan Aerospace Exploration Agency (JAXA), aiming to measure tropical rainfall. In general, the values estimated by the TRMM show a significant correlation with those measured on the ground, which explains their wide use in the world. To calculate the *R* factor values for the study area, we used the Rango–Arnoldus formula (Djoukbala et al. 2018; Rango and Arnoldus 1987; Sadiki et al. 2004). This formula is the most used and which requires only introducing monthly and annual precipitation whose expression is (Benselama et al. 2018):

$$logR = 1.74*log\sum\left(\frac{pi^2}{p}\right) + 1.29 \tag{2}$$

where Pi is the monthly precipitation and P is the annual precipitation in mm.

Soil erodibility (K) factor The *K* factor represents the influence of different soil properties on the slope's susceptibility to erosion. It is defined as the "average annual loss rate of rainfall" for a "standard condition of bare soil," which is recently increased with no conservation practice (Morgan 2005). The *K* factor essentially represents the soil loss that would occur on the USLE unit plot, with 22.1 m long, 1.83 m wide, and a slope of 9% (López-Vicente et al. 2008). Erodibility is closely related to the infiltration capacity of the soil, its structural stability, and its percentage of organic matter (Roose 1994).

Fig. 5 Soil erodibility map (*K*)

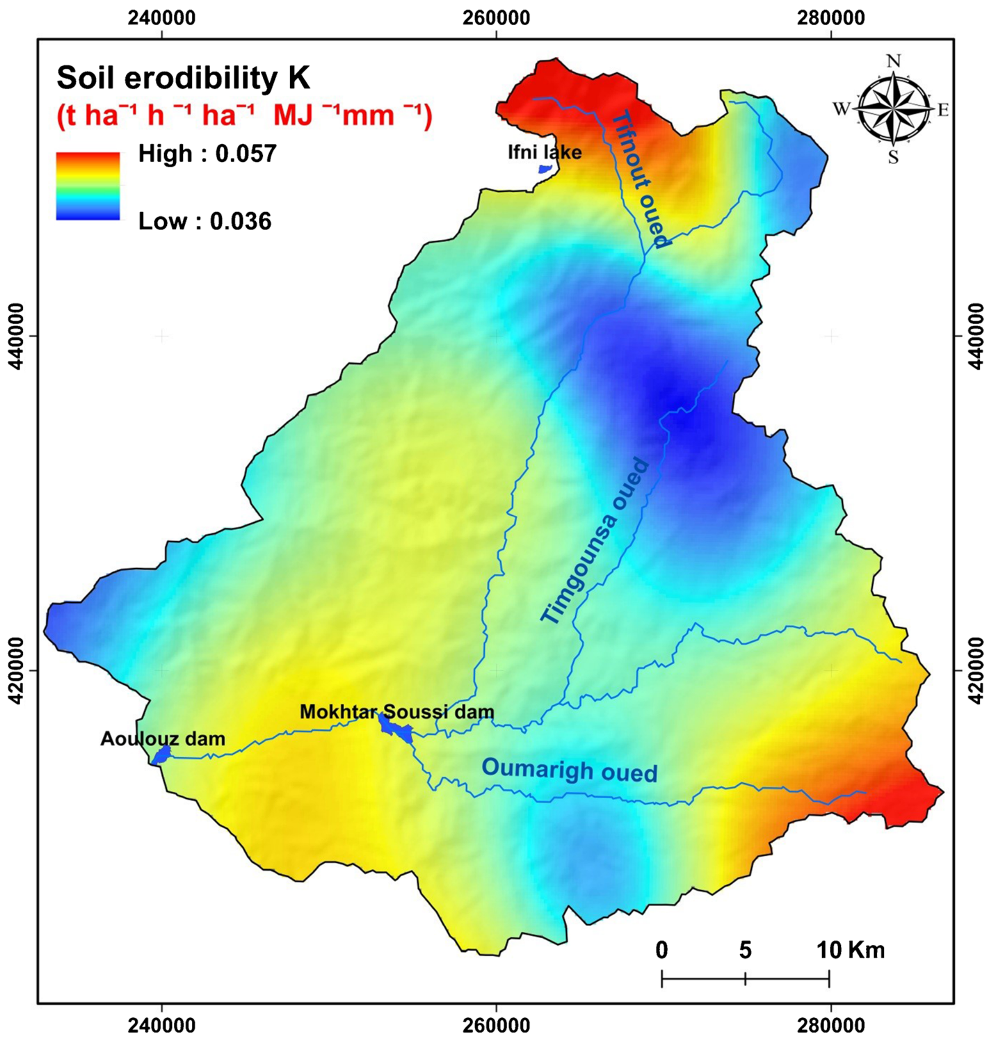

A very important role in the erodibility factor, the soil becomes easily erodible when the silty fraction increases with respect to clay and sand which constitute the more erodible fraction. Thus, in structurally stable soil with high organic matter content, the runoff rates decrease and, consequently, the rate of erosion (Kacem et al. 2018).

To develop the *K* factor map, a total of 24 soil samples were taken from the study area on October 28, 2018, and analyzed for their characteristics in the Laboratory of Applied Geology and Geo-Environment of the Faculty of Sciences at the University Ibn Zohr in Agadir, Morocco.

K factor values for the study area were calculated from the Williams equation (Nyesheja et al. 2019; Sharpley and Williams 1990; Williams and Singh 1995):

$$K\ rusle = f_{csand} * f_{cl-si} * f_{orgC} * f_{hisand} * 0.1317$$
$$f_{csand} = 0.2 + 0.3 exp\left(0.0256 * Sa * \left(1 - \frac{Si}{100}\right)\right) \tag{3}$$
$$f_{cl-si} = \left(\frac{Si}{Cl + Si}\right)^{0.3}$$
$$f_{orgC} = \left(1 - \frac{0.25 * C}{C + exp(3.72 - 2.95C)}\right)$$
$$f_{hisand} = \left(1 - \frac{0.7 * SN}{SN + exp\left(-5.51 + 22.9SN\right)}\right)$$

where:

Sa is sand %
Si is silt %
Cl is clay%
C is organic carbon %
SN is $1-\left(\frac{Sa}{100}\right)$.

Slope length (LS) factor This topographic factor influences strongly the importance of water erosion by its shape, inclination, and length. The LS factor is calculated by the combination of inclination and slope length. Several formulas allow

Fig. 6 Slope length (LS) map

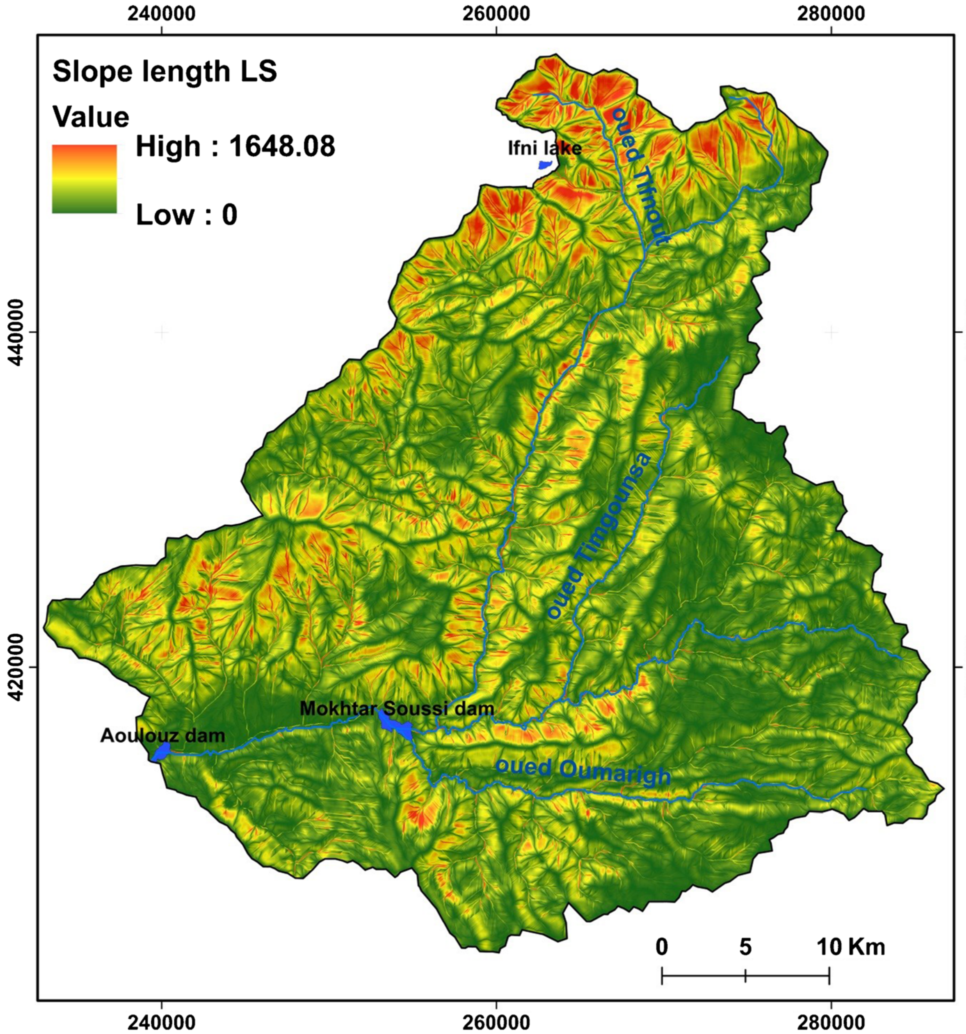

the evaluation of this factor from the numerical model of the ground, with a resolution of 30 m (David 1988; Kalman 1967; Wischmeier and Smith 1978).

To calculate the LS factor, we use the Mitasova equation where the adopted parameters, slope, and flow accumulations were computed from the digital elevation model (DEM) (Benavidez et al. 2018; Mitasova et al. 1996):

$$LS = (Pow(Flow\ accumulation * cell\ size)/22.1, 0.6) * Pow(sin(slope) * 0.01745/0.09, 1.3) \quad (4)$$

where LS is the length–slope steepness factor, cell size is the size of grid cell (for this study 30 m), and sin slope is the slope degree value in sin.

Cover and management (C) and conservation practice (P) factors The *C* and *P* factors are interdependent and can be extracted from land cover and land use map. In this study, to map the land cover of the study area, we processed a Landsat 8 OLI image (path/row 202/35) that was acquired in August 23, 2018. In their collected form from theUSGS website, the Landsat 8 OLI data are geometrically corrected, ortho-rectified, and radiometrically calibrated (see USGS site). The characteristics of the used data are given in Table 1.

Commonly, several algorithms have been used to correct the atmospheric effects on satellite data, including Dark object subtraction (DOS) and Fast Line-of-sight Atmospheric Analysis of Spectral Hypercubes (FLAASH). In this study, due to its simplicity and satisfactory results, we used the FLAASH algorithm to eliminate the effects of atmospheric scattering by subtracting from each band the value of the darkest pixel. Afterward, in order to map land cover and land use, we applied a supervised classification on three first components obtained from the principal component analysis (PCA) transformation, which commonly contain most information. The classification was achieved by using the maximum likelihood algorithm. All steps were achieved using ENVI software.

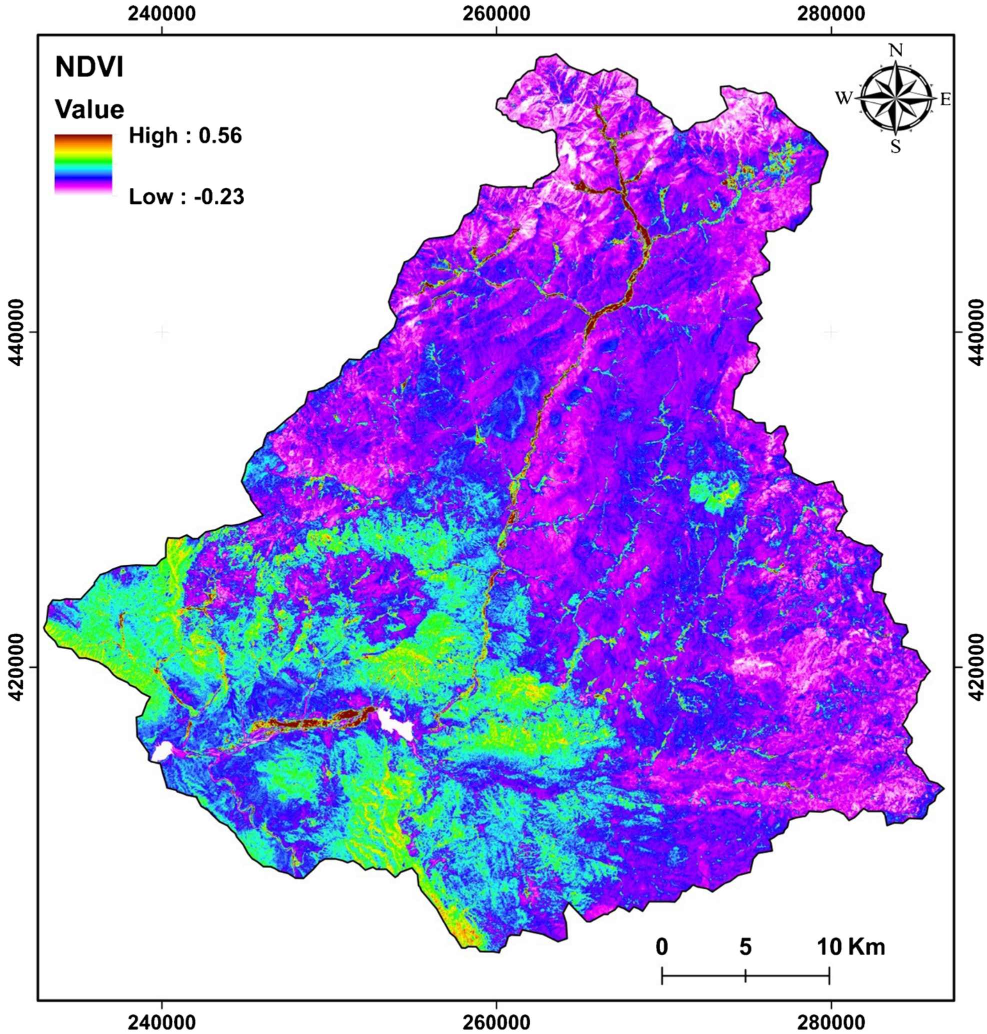

Fig. 7 NDVI map of the Tifnout Askaoun watershed

In order to evaluate the accuracy assessment of supervised classification outputs, the confusion table is widely used to express the proportionate reduction in error generated by a classification process compared with the error of a completely random classification (Aydda et al. 2019; Congalton 1991).

This table compares the ground truth data (real data) and classified data through assessing various statistics accuracies, including overall accuracy, user's accuracy, producer's accuracy, and Kappa coefficient.

Herein, we used Google Earth satellite images archive of the year 2019 to validate the obtained land cover and land use classified map. Practically, the obtained map was overlapped on Google Earth images to check the validity of each class. The overall accuracy of the obtained map is about 84%, and the Kappa coefficient is about 0.80, indicating a satisfactory result for best classification (Table 2).

Cover and management (C) Vegetation can intervene against surface water erosion in two main ways. First, it can prevent the ablation of the substrate. Then, it can promote the sedimentation by retaining the eroded sediments to the upstream part (Rey et al. 2004). Vegetation reduces also the energy of the surface runoff by acting as an interception of raindrops because of the aerial parts of the plants. This interception is a function of the density of the vegetative area and the structure of the plant cover. The vegetation also reduces surface runoff, by increasing the infiltration of the water (Cerdà 1998; Cosandey et al. 2000; Geddes and Dunkerley 1999).

The normalized difference vegetation index, called NDVI, is constructed from the red (R) and near-infrared (PIR) bands. The normalized vegetation index highlights the difference between the visible band of red and the near-infrared:

$$NDVI = \frac{(PIR - R)}{(PIR + R)} \quad (5)$$

This index is sensitive to the vigor and quantity of vegetation. NDVI values range from − 1 to + 1, with

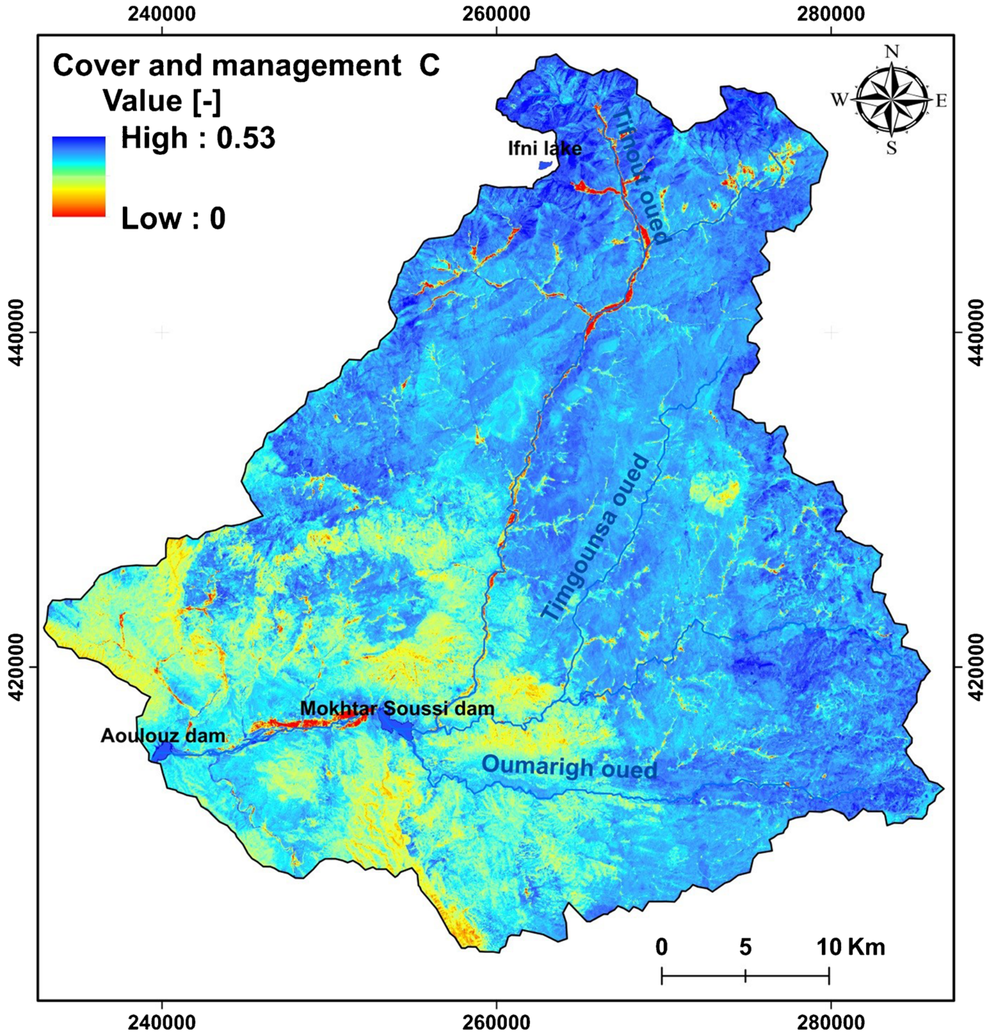

Fig. 8 Cover and management (C) map

negative values for surfaces other than plant covers, such as snow, water, or clouds, where red reflectance is greater than near-infrared. For bare soils, the reflectance is in the same order of magnitude in the red and the near-infrared, and then the NDVI has values close to 0. The vegetal formations have values of NDVI positive, generally between 0.1 and 0.7. The highest values correspond to the more dense vegetation cover.

Numerous empirical relationships or equations have been established to relate the values of NDVI to the values of factor C (Phinzi and Ngetar 2019). These equations have been applied in several studies around the world, namely, regression equation to calculate the C factor (Dutta et al. 2015; Moses 2017; Uddin et al. 2016) who used De jong (1994).

To map the C factor, we use a formula established by De Jong (1994), revised in 1998 (De Jong et al. 1998), where the NDVI factor is generated from the Landsat 8 OLI image:

$$C = 0.431 - 0.805 * NDVI \quad (6)$$

Conservation practice (P) factor P factor describes the relationship between soil erosion and the conservation practices adopted in the field. These control practices reduce the rate of soil degradation by reducing the potential for runoff erosion by influencing the drainage, concentration, velocity, and hydraulic forces of flows. In the absence of conservation measures, the value of P is 1.0 (Benavidez et al. 2018; Dutta et al. 2015; Phinzi and Ngetar 2019).

To map the P factor, values were assigned for each land use class, according to Table 3.

Results

R factor

The mean annual and monthly precipitation derived from TRMM data was used to map the R factor which is characterized by medium to high values ranging from 48.66 to 143.032

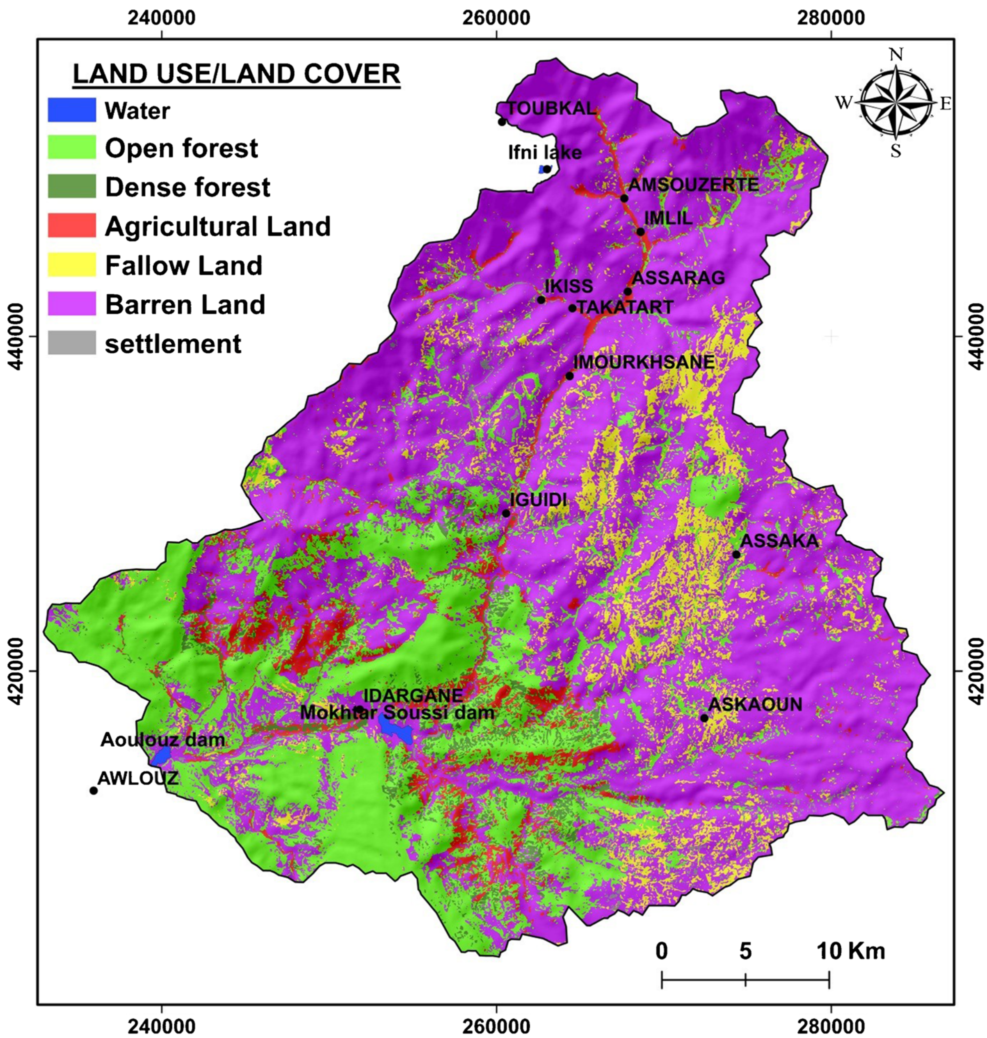

Fig. 9 Land use and land cover map

(MJ.mm.h^{-1} h^{-1} year^{-1}) and an average of 94.58 (MJ.mm.h^{-1} h^{-1} year^{-1}) for the whole study area (Fig. 4). The highest rainfall erosivity (R) values are observed in the high-altitude zone north of the study area, near the summit of Toubkal, and to the southeast in the mountain of Siroua in Askaoun.

K factor

The results of granulometric analyses of soil samples in the study area show the dominance of the sand followed by silt and low clay content, which gives a sandy silt texture for the majority of the analyzed samples. The dominant silt fraction compared to that of clays facilitates soil erosion in the Tifnout Askaoun watershed (Table 4). To evaluate the spatial variability of the K factor, several different interpolation methods were applied in ArcGIS 10.4.1 environment (such as Spline, inverse distance weighted (IDW)), but the ordinary kriging method based on Gaussian function was proved to be the most effective one for the production of the final erodibility map.

The kriging interpolation technique is the most used. It has the advantage of taking into account the distances between the data (the measurement points), the distances between the data and the target (the points for which we want to estimate the measurement), and the spatial structure (Alexakis et al. 2013; Bouderbala et al. 2019).

The results obtained for the K factor of the Tifnout Askaoun watershed vary from 0.03 (t ha MJ^{-1} mm^{-1}) for the most resistant soils to 0.05 (t ha MJ^{-1} mm^{-1}) for the most erodible soils with an average of 0.044 (t ha MJ^{-1} mm^{-1}). The K factor map shows that the highest K values are located in the south east near the Askaoun zone, in the north east near the Ifni lake, and in the south around the Mokhtar Soussi and Aoulouz dams (Fig. 5).

LS factor

To mapping, the slope length (LS) factor by the Mitasova equation, the slope steepness values, and flow accumulation derived from DEM were used. The slope length factor (LS)

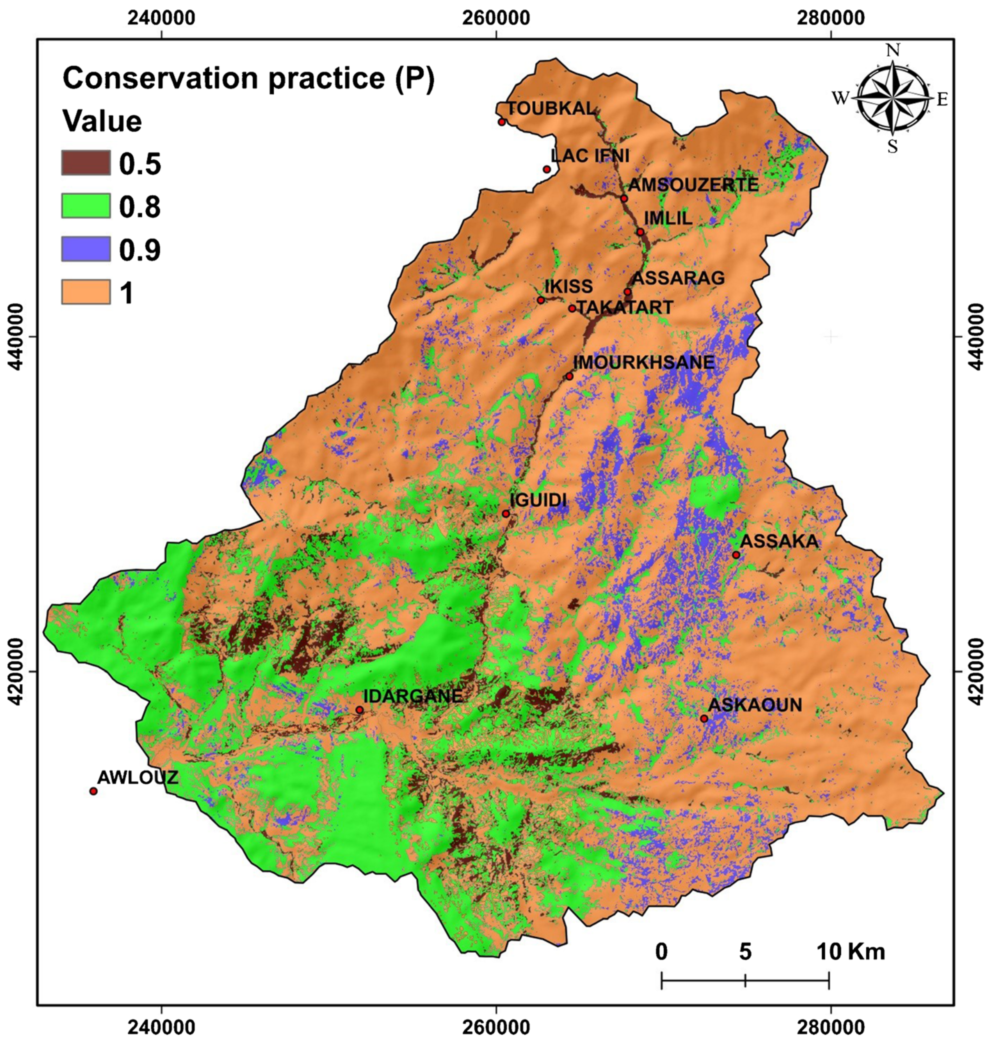

Fig. 10 Conservation practice (P) map

varies from 0 to 1648.08 with an average value of 15.09 (Fig. 6). It is very strong at the high altitudes of the High Atlas Mountains where it exceeds 1500 near Lake Ifni.

C factor

The identification of crop types at the plot level is difficult from the satellite image; NDVI has been used as a substitute of Landsat image for estimating *C* factor in the Tifnout Askaoun watershed (Fig. 7). The values obtained for the *C* factor range from 0 to 0.53 with an average of 0.23 (Fig. 8).

The higher values of C factor are observed in the more unprotected soil. Areas without vegetation cover to the north-east and southeast present a high potential risk of soil erosion concerning *C* factor, while areas of dense vegetation cover to the south around the Mokhtar Soussi and Aoulouz dams show low sensitivity to soil erosion.

Table 5 Annual soil erosion rate distribution in the Tifnout Askaoun watershed

Soil loss (t/ha/year)	Percent of global area
< 5	27.06%
5–25	51.96%
25–50	13.97%
50–75	3.64%
> 75	3.33%

P factor

From the land use map, we noticed that 58% of the study area is occupied by the barren land class, followed by an open forest class with 28%. Agricultural and fallow land occupies 5 and 8%, respectively (Fig. 9). The values of *P* are assigned for each land use class according to Table 3. The map of the *P* factor shows that the majority of the study area displays values between 0.9 and 1, indicating the dominance of the barren land except in the south at Aouzioua (Fig. 10).

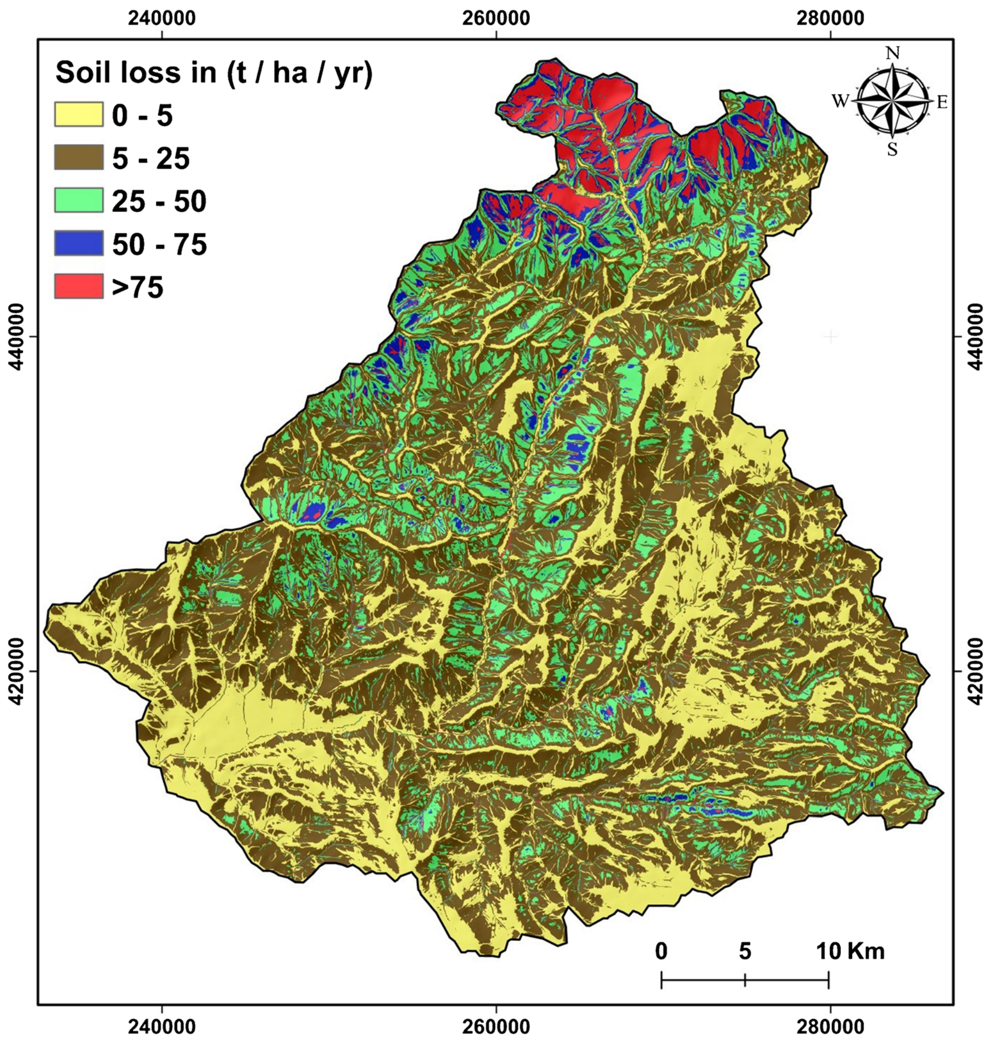

Fig. 11 Map of RUSLE soil erosion in Tifnout Askaoun watershed

Evaluation of the soil loss

Overlaying the raster data layers representing erosion factors *R*, *K*, *C*, LS, and *P* in a GIS environment results in a map of the distribution of the annual soil losses in the Tifnout Askaoun watershed which is a mountainous area in southern Morocco (Fig. 11). The composite map highlights six classes which are given in Table 5. The result obtained indicates an estimated annual erosion rate ranging from 0 to 152.33 and an average of about 14.44 t/ha/year for the entire watershed studied. The results show that more than 20% of the investigated area has an erosion rate greater than 25 t/ha/year. Areas with a very high risk of erosion are located in the north east of the study area (High Atlas), while low-risk areas are located in the south and south east (Anti-Atlas) and along the Tifnout Valley.

Discussion

The tolerance thresholds for erosion in a temperate humid climate vary between 2.5 and 12.5 t/ha/year (Klingebiel and Montgomery 1966; USDA 1951), and this tolerance is lower in Mediterranean countries such as Morocco because of the pedogenesis which is much slower. Therefore, the values of soil losses cited above greatly exceed what pedogenesis can produce under current climatic conditions.

Table 6 Sedimentation observed in the dams of the study area

Dam	Date	Stockage volume (Mm^3)	Observed sedimentation ($Mm^3. yr^{-1}$)	Source
Aoulouz	1991	110.00	1.20	Badraoui and Hajji 2001
Mokhtar Soussi	2002	50.00	1.55	Elmouden et al. 2017

Table 7 Statistics of calculated soil erosion and adopted factors

	A: soil erosion in (t/ha/year)				*C*				*R*				*K*				LS			
W	Min	Max	Mean	STD	Min	Max	Mean	STD	Min	Max	Mean	STD	Min	Max	Mean	STD	Min	Max	Mean	STD
1	0	778.28	48.05	47.96	0	0.36	0.26	0.05	91.86	136.80	124.17	10.57	0.0300	0.0499	0.0457	0.0031	0	489.29	29.96	26.81
2	0	310.86	27.38	25.04	0	0.34	0.25	0.03	89.31	114.44	100.58	4.71	0.0344	0.0490	0.0425	0.0023	0	260.53	27.26	21.44
3	0	577.847	12.46	13.23	0	0.32	0.25	0.03	80.52	113.18	90.68	7.51	0.0300	0.0472	0.0403	0.0045	0	241.08	15.95	16.27
4	0	256.51	22.15	19.14	0	0.33	0.24	0.03	86.09	110.82	100.78	5.99	0.0400	0.0496	0.0434	0.0030	0	187.69	20.12	15.95
5	0	484.55	26.03	23.49	0	0.33	0.25	0.02	98.55	116.29	108.30	3.54	0.0414	0.0499	0.0453	0.0020	0	324.17	21.80	18.98
6	0	476.51	18.82	17.44	0	0.31	0.24	0.02	99.67	123.94	113.13	5.15	0.0407	0.0468	0.0433	0.0013	0	373.94	15.38	15.03
7	0	1371.58	20.96	32.81	0	0.33	0.25	0.04	84.72	114.56	99.29	6.45	0.0313	0.0444	0.0404	0.0015	0	1072.70	20.60	31.89
8	0	322.04	11.34	10.03	0	0.33	0.25	0.25	77.72	93.28	83.06	3.13	0.0389	0.0475	0.0434	0.0015	0	385.02	13.42	13.01
9	0	469.93	7.73	9.54	0	0.34	0.25	0.08	77.97	101.66	85.98	5.32	0.0424	0.0463	0.0442	0.0007	0	441.02	8.33	9.84
10	0	129.41	6.83	5.84	0	0.31	0.18	0.03	48.66	64.50	53.58	3.17	0.0411	0.0446	0.0433	0.0006	0	321.45	20.50	16.87
11	0	352.05	12.08	12.91	0	0.31	0.21	0.04	53.75	92.31	66.38	9.08	0.0414	0.0468	0.0443	0.0010	0	549.20	23.90	22.74
12	0	657.73	14.32	17.54	0	0.33	0.22	0.04	70.95	103.47	88.61	7.06	0.0417	0.0499	0.0467	0.0017	0	677.96	19.09	21.08
13	0	1615.23	13.96	24.40	0	0.45	0.21	0.04	84.22	104.18	91.83	3.94	0.0421	0.0499	0.0468	0.0468	0	1648.07	19.85	29.15
14	0	721.39	14.97	20.53	0	0.32	0.20	0.04	86.55	108.11	94.50	3.33	0.0409	0.0466	0.0436	0.0010	0	643.32	21.16	24.73
15	0	368.60	9.00	12.65	0	0.36	0.26	0.02	87.74	116.24	103.97	6.54	0.0400	0.0499	0.0457	0.0020	0	438.50	6.95	10.27
16	0	242.93	4.95	8.31	0	0.53	0.21	0.04	49.67	79.29	62.96	7.80	0.0400	0.0499	0.0458	0.0026	0	302.23	9.74	13.95
17	0	563.95	6.82	11.21	0	0.14	0.19	0.06	70.11	88.14	78.53	4.61	0.0454	0.0499	0.0482	0.0011	0	364.39	11.76	13.23
18	0	208.95	12.42	12.97	0	0.41	0.21	0.03	72.79	114.87	94.12	9.37	0.0400	0.0476	0.0436	0.0017	0	2.86.00	17.01	17.60
19	0	343.37	12.73	13.64	0	0.32	0.26	0.02	102.60	128.03	117.58	4.00	0.0432	0.0486	0.0467	0.0008	0	295.97	9.54	10.38
20	0	177.65	7.68	8.21	0	0.33	0.21	0.03	55.51	73.42	65.23	4.29	0.0437	0.0480	0.0467	0.0007	0	231.74	13.04	12.94
21	0	171.38	7.87	8.94	0.04	0.30	0.20	0.03	68.81	91.05	76.45	5.68	0.0409	0.0465	0.0446	0.0011	0	317.89	15.33	15.64
22	0	482.39	9.76	13.60	0	0.31	0.23	0.02	79.45	128.07	99.73	11.46	0.0400	0.0466	0.0433	0.0013	0	492.00	12.95	16.75
23	0	683.02	16.31	20.89	0	0.34	0.25	0.02	103.49	143.03	128.06	7.25	0.0442	0.0499	0.0473	0.0012	0	579.73	10.61	14.26

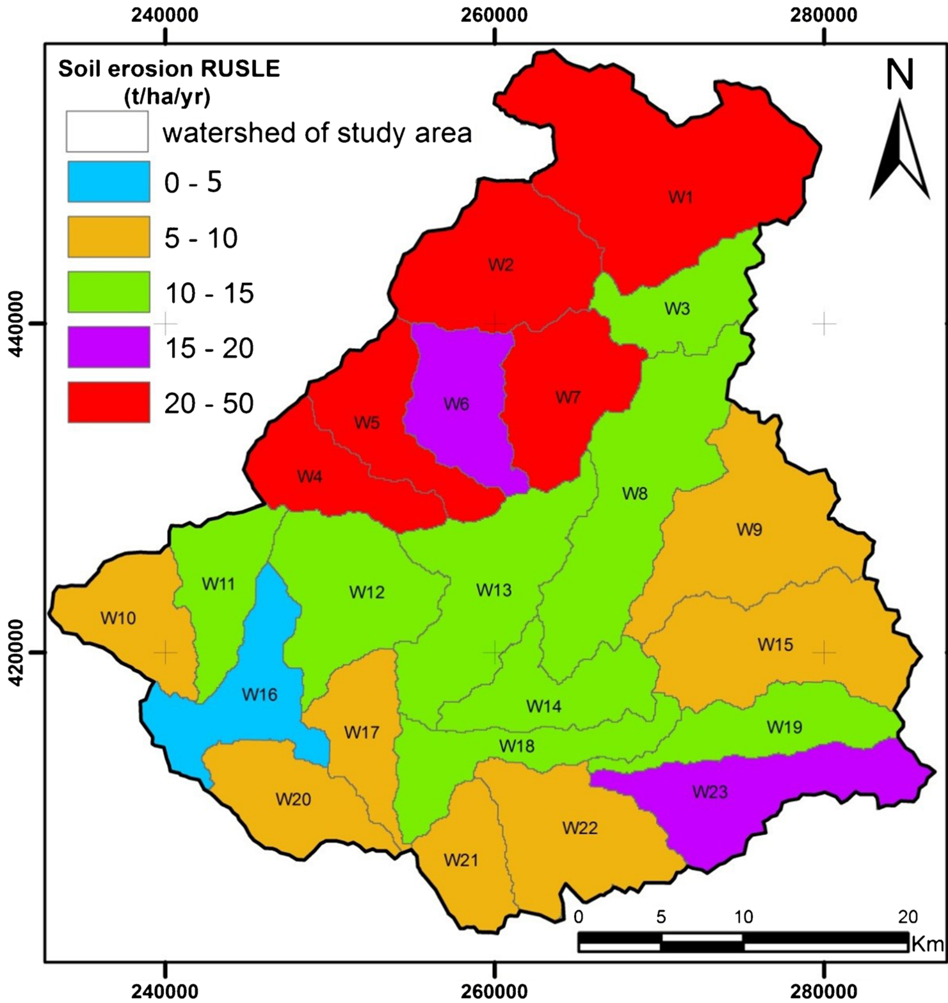

Fig. 12 Subdivision of the study area according to the calculated erosion rate. Wx indicates sub-catchment in the study area

The soil loss rate obtained is higher than the tolerance limit of soil loss for High Atlas set between 5 and 10 t/ha/year (El-Ghanam and El-Ghozoli 2003; Ouassou et al. 2006; Snoussi 1988).

The comparison of our results to the study carried out by Gourfi et al. (2018) covering the whole of Morocco shows relative reliability of the model applied. It demonstrated an annual average rate greater than 20 t/ha/year for the whole country with a resolution of 1 km. Sedimentation and siltation calculations in the two dams (Mokhtar Soussi and Aoulouz) of the study area indicate that the two reservoirs are threatened by a very high rate of siltation (Table 6).

Table 8 Correlation matrix of soil erosion rate calculated by RUSLE and adopted factors

	A	*C*	*R*	*K*	LS
A	1	0.50	0.63	−0.11	0.72
C		1	0.73	−0.20	−0.05
R			1	0.04	0.08
K				1	−0.30
LS					1

The inequality of the distribution of soil losses in the different zones of the Tifnout Askaoun watershed is due to the variability of the different factors from one place to another. We subdivided the study area into 23 sub-catchments and noted that those located in the north and on the southern flank of the High Atlas Mountains show a higher erosion rate compared to those located along the Tifnout Valley and in the Askaoun zone (Fig. 12). The catchment (W1) of Toubkal is threatened by a very strong water erosion of an average of 48.05 (t/ha/year) because of the scarcity of the vegetation cover and the steep slope. We note that the w1, w2, w4, w5, and w7 sub-basins in the High Atlas show a risk of erosion from high to very high. To test the correlation between the input factors and the result obtained by the RUSLE model, we have calculated the characteristics of each catchment (Table 7).

In general, all factors of the revised universal equation (topography, erodibility, climatology, and vegetation cover) do not show the same correlation with the annual erosion value (*A*) calculated by the RUSLE equation (Table 8) and (Fig. 13).

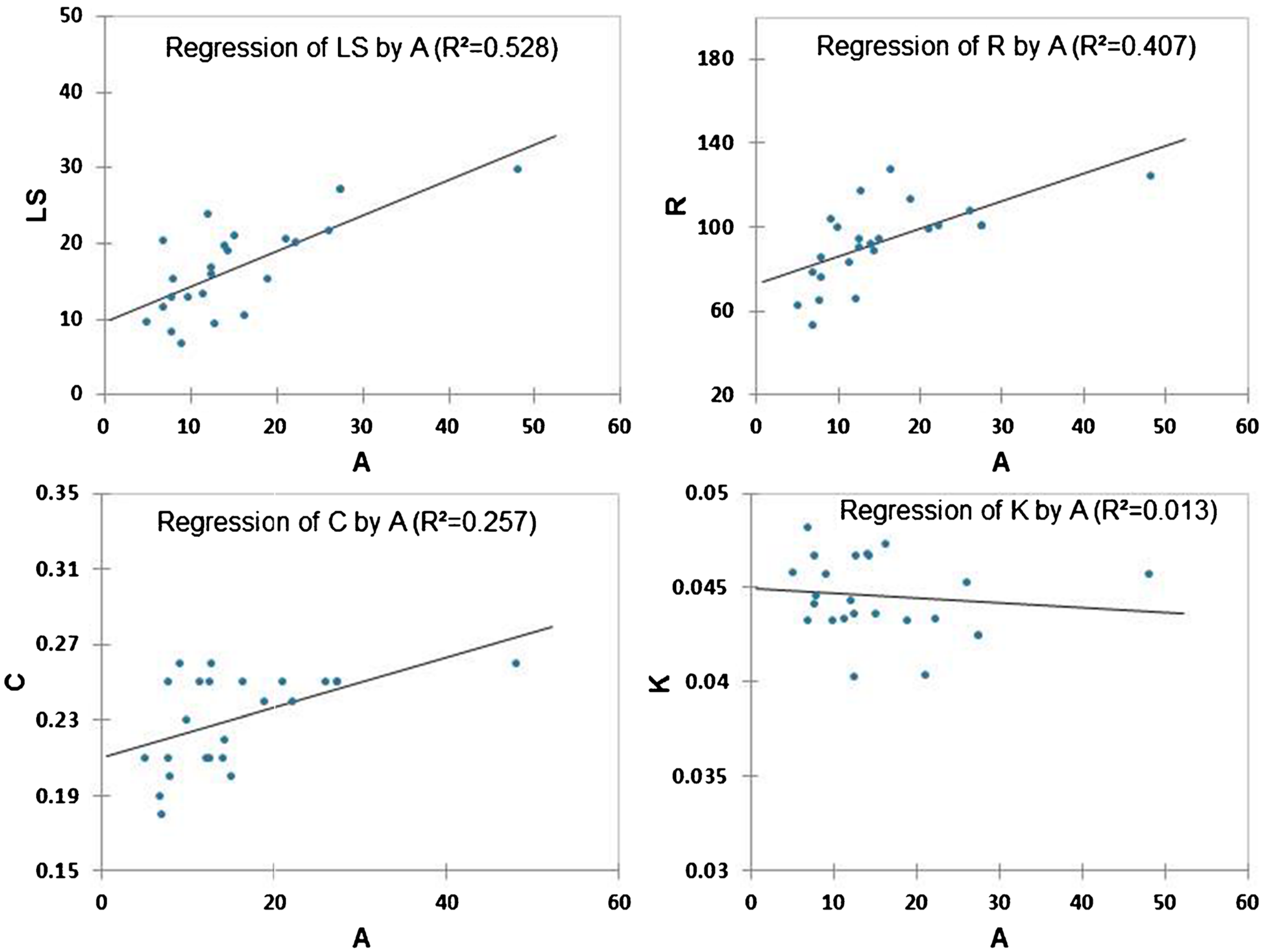

Fig. 13 Regression of LS, *R*, *C*, and *K* factors by *A* soil erosion

The correlation matrix shows that the factor LS indicates the best correlation with the sensitivity to water erosion with a correlation coefficient of $r = 0.72$. This means that the LS dominates and controls the process of water erosion, followed by the *R* and *C* factors. The *K* factor shows a negative correlation $r = 0.11$ explained by the impossibility of sampling the soil in some inaccessible locations.

The priority for intervention against erosion in each sub-catchment is to prioritize an action plan against water erosion. Prioritizing the action plan in the sub-catchments requires a strategy that includes two main conditions, namely:

- The average annual soil loss rate calculated in each sub-catchment
- The protection of the Mokhtar Soussi and Aoulouz dams against the acceleration of their siltation, by considering the distance between the outlet of each sub-basin and the reservoir of the dam concerned

Table 9 Decision matrix for priority intervention in each sub-catchment

A (t/ha/an)	Distance/dams (Km)				
	> 30	25–30	20–25	10–20	0–10
0–5	Not urgent	Low	Low	Low	Low
5–10	Low	Low	Medium	Medium	Medium
10–15	Low	Medium	Medium	High	High
15–20	Medium	Medium	High	High	Very high
20–50	Medium	High	High	Very high	Very high

In this context, a decision matrix has been developed to define the intervention priority levels for each sub-catchment. Five classes have been designed ranging from non-urgent to very urgent action (Tables 9 and 10).

Among the 23 sub-catchments of the study area, it turns out that sub-basin number 5 located to the north of the study area shows a very high priority to develop and implement a more urgent action plan, given that its distance from the Mokhtar Soussi dam is less than 20 km and its average annual soil loss is estimated at 26.03 t/ha/year (Fig. 14).

Table 10 Priority classes of the 23 sub-basins of the Tifnout Askaoun catchment

Sub-catchment	Soil erosion in (t/ha/year)	Distance/dams (Km)	Priority
3	12.46	32	Low
16	4.95	0	Low
17	6.82	31.76	Low
1	48.05	35.42	Medium
2	27.38	32.97	Medium
9	7.73	21.87	Medium
10	6.83	3.52	Medium
15	9.00	21.87	Medium
20	7.68	3.40	Medium
21	7.87	8.80	Medium
22	9.76	8.80	Medium
4	22.15	24.98	High
6	18.82	19.51	High
7	20.96	21.36	High
8	11.34	13.79	High
11	12.08	3.52	High
12	14.32	9.88	High
13	13.96	0	High
14	14.97	2.76	High
18	12.42	0	High
19	12.73	17.33	High
23	16.31	17.33	High
5	26.03	19.51	Very high

The high-priority watershed sub-basins cover 71% of the study area; there are 11 sub-catchments (4, 6, 7, 8, 11, 12, 13, 14, 18, 19, 23) classified as urgent priority with average soil losses between 11.34 and 22.15 t/ha/year and distances between 0 and 24.98. They are mainly elongated in the central part of the watershed.

Despite the high erosion values estimated for some sub-watershed, the intervention priority matrix assigned non-urgent priority to these because of the great distances from the reservoirs of the dams in the study area, but this does not prevent these sub-basins from benefiting from intervention against the phenomenon of water erosion.

Conclusions

It emerges from the application of the RUSLE model in the Tifnout Askaoun watershed that the *R* climate of the region has a variant aggressiveness of 48.66 to 143,032 units/year with an average of 94.58 units/year and an erodibility of soils *K* from 0, 03 to 0.05 with an average of the order of 0.04 and a topographic factor LS varying from 0 to 1648.08 with an average of 17.05 which is due to the nature of the very rugged terrain and the steep slopes of the High Atlas and Anti-Atlas mountains.

The Landsat image allowed us through the NDVI to map the *C* factor which varies from 0 to 0.53 with an average of 0.23 and which characterizes the protection conferred on the soil by the vegetation cover and on the basis on the mapping of the land cover; the values obtained for the *P* factor vary from 0.9 to 1 with an average of 0.85. This estimated rate of erosion represents a major risk for water reservoirs storage of the Mokhtar Soussi and Aoulouz dams. The result obtained by superimposing the five parameters of the RUSLE equation in a GIS environment indicates an annual average soil erosion of 14.44 t/ha/year for the studied area.

The results obtained show that the High Atlas Mountains, characterized by an active alpine neotectonics which accelerates erosion, show a greater rate of soil degradation especially in areas with marl–limestone lithology. However, the Anti-Atlas Mountains with stable Pan-African tectonics present medium erosion except at the high altitudes where the alteration of the magmatic rocks is intensely producing granitic sand easily transported.

The proposed intervention priority matrix enabled us to distinguish a sub-catchment area of very high intervention priority (sub-catchments area N°5) and eleven sub-catchments showing high priority (sub-catchments N°, 4,

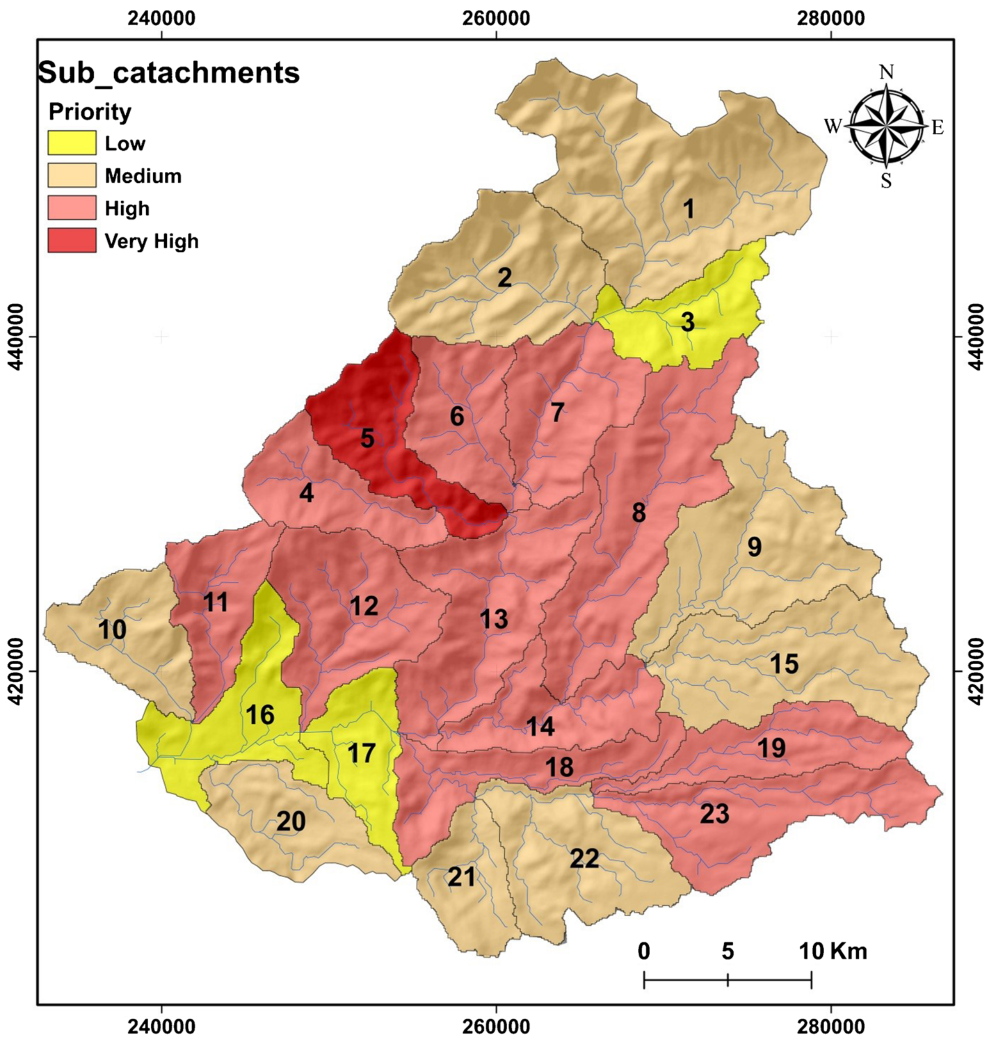

Fig. 14 Priority (from low to very high) map of the sub-catchments of the study area. The number indicates the sub-catchment

6, 7, 8, 11, 12, 13, 14, 18, 19, and 23). The use of TRMM data will be a valuable method solution to solve the problem of precipitation data in Morocco.

Nevertheless, it is advisable to keep a critical sense with regard to these results because the RUSLE model in its primary objective was intended to be used in areas with low slope and only applies to sheet erosion since the source of energy is rain, so it does not apply to linear erosion. These results can be combined with those obtained by other methods of evaluating water erosion. For more precision, other methods are interesting, particularly radio-isotopic methods, SWAT model (Soil Water Assessment Tools), and the SAM model.

Acknowledgements We thank NASA and the Hydraulic Agency of Souss–Massa Basin in Morocco for providing the data. This study is carried out as part of the CHARISMA project with the support of the Academy Hassan II of Sciences and Technology. We would like to thank the chief editor and reviewers of the Arabian Journal of Geosciences for their constructive comments. We also thank professors Brahim Souss and Ali Aydda for their help with the English editing.

Declarations

Conflict of interest The authors declare no competing interests.

References

Abuzied SM, Alrefaee HA (2019) Spatial prediction of landslide-susceptible zones in El-Qaá area, Egypt, using an integrated approach based on GIS statistical analysis. Bull Eng Geol Environ 78(4):2169–2195. https://doi.org/10.1007/s10064-018-1302-x

Abuzied S, Ibrahim S, Kaiser M, Saleem T (2016a) Geospatial susceptibility mapping of earthquake-induced landslides in Nuweiba area, Gulf of Aqaba, Egypt. J Mt Sci 13(7):1286–1303. https://doi.org/10.1007/s11629-015-3441-x

Abuzied S, Yuan M, Ibrahim S, Kaiser M, Saleem T (2016b) Geospatial risk assessment of flash floods in Nuweiba area, Egypt. J Arid Environ 133:54–72. https://doi.org/10.1016/j.jaridenv.2016.06.004

Alexakis DD, Hadjimitsis DG, Agapiou A (2013) Integrated use of remote sensing, GIS and precipitation data for the assessment of soil erosion rate in the catchment area of "Yialias" in Cyprus. Atmos Res 131:108–124. https://doi.org/10.1016/j.atmosres.2013.02.013

Aydda A, Althuwaynee OF, Ahmed A, Abdellah A (2019) Evolution of sand encroachment using supervised classification of Landsat data during the period 1987–2011 in a part of Laâyoune-Tarfaya basin of Morocco. Geocarto Int 34(13):1514–1529. https://doi.org/10.1080/10106049.2018.1493154

Badraoui A, Hajji A (2001) Envasement des retenues de barrages. La Houille Blanche 6-7:72–75. https://doi.org/10.1051/lhb/2001073

Belkacim S, Gasquet D, Liégeois JP, Arai S, Gahlan HA, Ahmed H, Ishida Y, Ikenne M (2017) The Ediacaran volcanic rocks and associated mafic dykes of the Ouarzazate Group (Anti-Atlas, Morocco): clinopyroxene composition, whole-rock geochemistry and Sr-Nd isotopes constraints from the Ouzellarh-Siroua salient (Tifnoute valley). J Afr Earth Sci 127:113–135. https://doi.org/10.1016/j.jafrearsci.2016.08.002

Benavidez R, Jackson B, Maxwell D, Norton K (2018) A review of the (Revised) Universal Soil Loss Equation ((R)USLE): with a view to increasing its global applicability and improving soil loss estimates. Hydrol Earth Syst Sci 22:6059–6086. https://doi.org/10.5194/hess-22-6059-2018

Benselama O, Mazour M, Hasbaia M, Djoukbala O, Mokhtari S (2018) Prediction of water erosion sensitive areas in Mediterranean watershed, a case study of Wadi El Maleh in north-west of Algeria. Environ Monit Assess 190:735. https://doi.org/10.1007/s10661-018-7117-1

Bonn F (1998) La spatialisation des modèles d'érosion des sols à l'aide de la télédétection et des SIG: possibilités, erreurs et limites. Sécheresse 9(3):185–192

Bouchaou L, Michelot JL, Vengosh A, Hsissou Y, Qurtobi M, Gaye CB, Bullen TD, Zuppi GM (2008) Application of multiple isotopic and geochemical tracers for investigation of recharge, salinization, and residence time of water in the Souss–Massa aquifer, southwest of Morocco. J Hydrol 352(3-4):267–287. https://doi.org/10.1016/j.jhydrol.2008.01.022

Bouderbala D, Souidi Z, Hamimed A, Bouamar B (2019) Estimativa da erosividade da chuva por mapeamento na bacia de Macta (Argélia). Rev Bras Cartogr 71(1):274–294. https://doi.org/10.14393/rbcv71n1-2218

BouKheir R, Cerdan O, Abdallah C (2006) Regional soil erosion risk mapping in Lebanon. Geomorphology 82(3–4):347–359. https://doi.org/10.1016/j.geomorph.2006.05.012

Cerdà A (1998) The influence of aspect and vegetation on seasonal changes in erosion under rainfall simulation on a clay soil in Spain. Can J Soil Sci 78(2):321–330. https://doi.org/10.4141/S97-060

Chafai A, Brahim N, Shimi NS (2020) Mapping of water erosion by GIS/RUSLE approach: watershed Ayda river Tunisia study. Arab J Geosci 13:810. https://doi.org/10.1007/s12517-020-05774-0

Choubert G (1947) L'accident majeur de l'Anti-Atlas. C R Acad Sci, Paris 224:1172–1173

Congalton RG (1991) A review of assessing the accuracy of classifications of remotely sensed data. Remote Sens Environ 37(1):35–46. https://doi.org/10.1016/0034-4257(91)90048-B

Cosandey C, J-F Didon L, Martin C (2000) Forêts et écoulements. Etude des processus responsables des modifications du bilan d'écoulement annuel à l'occasion d'une coupe forestière. Forêt Méditerranéenne 21(2):154–155

Dai Z, Feng X, Zhang C, Shang L, Qiu G (2013) Assessment of mercury erosion by surface water in Wanshan mercury mining area. Environ Res 125:2–11. https://doi.org/10.1016/j.envres.2013.03.014

David W P (1988) Soil and water conservation planning: policy issues and recommendations. J Philippine Dev 15(26):47–84

De Jong SM (1994) Derivation of vegetative variables from a Landsat TM image for modelling soil erosion. Earth Surf Process Landf 19(2):165–178. https://doi.org/10.1002/esp.3290190207

De Jong SM , Brouwer LC, Riezebos Ht (1998) Erosion hazard assessment in the La Peyne catchment, France. Working paper DeMon-2 Project, University of Utrecht

Djoukbala O, Mazour M, Hasbaia M, Benselama O (2018) Estimating of water erosion in semiarid regions using RUSLE equation under GIS environment. Environ Earth Sci 77:345. https://doi.org/10.1007/s12665-018-7532-1

Dutta D, Das S, Kundu A, Taj A (2015) Soil erosion risk assessment in Sanjal watershed, Jharkhand (India) using geo-informatics, RUSLE model and TRMM data. Model. Earth Syst Environ 1:37. https://doi.org/10.1007/s40808-015-0034-1

EL Haibi H, EL Hadi H, Tahiri A, Martínez Poyatos D, Gasquet D, Pérez-Cáceres I, González Lodeiro F, Mehdioui S (2020) Geochronology and isotopic geochemistry of Ediacaran high-K calc-alkaline felsic volcanism: an example of a Moroccan perigondwanan (Avalonian) remnant in the El Jadida horst (Mazagonia). J Afr Earth Sci 163: 103669. https://doi.org/10.1016/j.jafrearsci.2019.103669

El-Ghanam MMM, El-Ghozoli MA (2003) Remediation role of humic acid on faba bean plants grown on sandy lead polluted soil. Ann Agric Sci Moshtohor 41(14):1811–1826

Ellison WD (1946) Soil detachment and transportation. Soil Conserv 11(8):179–190

Elmouden A, Alahiane N, El Faskaoui M, El Morjani ZEA (2017) Dams siltation and soil erosion in the Souss–Massa river basin. In: Choukr-Allah R, Ragab R, Bouchaou L, Barceló D (eds) The Souss-Massa River Basin, Morocco, The Handbook of Environmental Chemistry. Springer International Publishing, Cham, pp 95–120. https://doi.org/10.1007/698_2016_70

Engel BA, Srinivasan R, Arnold J, Rewerts C, Brown SJ (1993) Nonpoint source (NPS) pollution modeling using models integrated with geographic information systems (GIS). Water Sci Technol 28(3–5):685–690. https://doi.org/10.2166/wst.1993.0474

Ennih N, Liégeois JP (2001) The Moroccan Anti-Atlas: the West African craton passive margin with limited Pan-African activity. Implications for the northern limit of the craton. Precambrian Res 112(3–4):289–302. https://doi.org/10.1016/S0301-9268(01)00195-4

Enters T (1998) Methods for the economic assessment of the on-and off-site impacts of soil erosion international board for soil research and management. issues in sustainable land management no. 2. IBSRAM, Bangkok

Foucault A, Raoult JF (1995) Dictionnaire de géologie (4ème édition). Masson, Paris

Geddes N, Dunkerley D (1999) The influence of organic litter on the erosive effects of raindrops and of gravity drops released from desert shrubs. CATENA 36(4):303–313. https://doi.org/10.1016/S0341-8162(99)00050-8

Gentil L (1905) Observations géologiques dans le sud marocain. CR Somm Soc Géol Fr 5:521–523

Gourfi A, Daoudi L, Shi Z (2018) The assessment of soil erosion risk, sediment yield and their controlling factors on a large scale: Example of Morocco. J Afr Earth Sci 147: 281-299. https://doi.org/10.1016/j.jafrearsci.2018.06.028

Hoepffner C, Soulaimani A, Piqué A (2005) The Moroccan Hercynides. J Afr Earth Sci 43(1-3):144–165. https://doi.org/10.1016/j.jafrearsci.2005.09.002

Kacem L, Agoussine M, Igmoullan B, Amar H, Mokhtari S (2018) Mapping soil erosion risk using RUSLE, GIS, remote sensing methods: a case of mountainous sub-watershed, Ifni Lake and high valley of Tifnoute (High Moroccan Atlas). J Geogr Environ Earth Sci Int 14(2):1–11. https://doi.org/10.9734/JGEESI/2018/40322

Kalman R (1967) Essai d'évaluation pour le pré-Rif du facteur couverture végétale de la formule de Wischmeier de calcul de l'érosion. In: Rapport pour l'administration de la forêt et d'eau, Rabat, pp 1–12

Khan A, Govil H (2020) Evaluation of potential sites for soil erosion risk in and around Yamuna River flood plain using RUSLE. Arab J Geosci 13:707. https://doi.org/10.1007/s12517-020-05646-7

Kirkby MJ, Abrahart R, McMahon MD, Shao J, Thornes JB (1998) MEDALUS soil erosion models for global change. Geomorphology 24(1):35–49. https://doi.org/10.1016/S0169-555X(97)00099-8

Klingebiel AA, Montgomery PH (1966) Land-capability classification. Washington, DC. US Department of agriculture, soil conservation service

Kouli M, Soupios P, Vallianatos F (2009) Soil erosion prediction using the Revised Universal Soil Loss Equation (RUSLE) in a GIS framework, Chania, Northwestern Crete, Greece. Environ Geol 57:483–497. https://doi.org/10.1007/s00254-008-1318-9

López-Vicente M, Navas A, Machin J (2008) Identifying erosive periods by using RUSLE factors in mountain fields of the Central Spanish Pyrenees. Hydrol Earth Syst Sci 12:523–535. https://doi.org/10.5194/hess-12-523-2008

Lu D, Li G, Valladares GS, Batistella M (2004) Mapping soil erosion risk in Rondônia, Brazilian Amazonia: using RUSLE, remote sensing and GIS. Land Degrad Dev 15(5):499–512. https://doi.org/10.1002/ldr.634

Mahala A (2018) Soil erosion estimation using RUSLE and GIS techniques—a study of a plateau fringe region of tropical environment. Arab J Geosci 11:335. https://doi.org/10.1007/s12517-018-3703-3

Michard A, Soulaimani A, Hoepffner C, Ouanaimi H, Baidder L, Rjimati EC, Saddiqi O (2010) The South-Western Branch of the Variscan Belt: Evidence from Morocco. Tectonophysics 492(1-4):1–24. https://doi.org/10.1016/j.tecto.2010.05.021

Missenard Y (2006) Le relief des Atlas Marocains: contribution des processus asthénosphériques et du raccourcissement crustal, aspects chronologiques. PhD Thesis, Cergy-Pontoise University

Mitasova H, Hofierka J, Zlocha M, Iverson LR (1996) Modelling topographic potential for erosion and deposition using GIS. Int J Geogr Inf Syst 10(5):629–641. https://doi.org/10.1080/02693799608902101

Morgan RPC (2005) Soil erosion and conservation. Blackwell Publishing, National Soil Resources Institute, Cranfield University

Morgan RPC, Quinton JN, Rickson RJ (1990) Structure of the soil erosion prediction model for the European community Proceedings of International Symposium on Water Erosion, Sedimentation and Resource Conservation, Central Soil and Water Conservation Research and Training Institute, CSWCRTI, Dehradun, India 49-59

Moses AN (2017) GIS-RUSLE interphase modelling of soil erosion hazard and estimation of sediment yield for river Nzoia basin in Kenya. J Remote Sens GIS 6(3):1–13. https://doi.org/10.4172/2469-4134.1000205

Moukhchane M (2002) Différentes méthodes d'estimation de l'érosion dans le bassin versant du Nakhla (Rif Occidental, Maroc). Bull Res Eros 21:255–266

Naqvi HR, Mallick J, Devi LM, Siddiqui MA (2013) Multi-temporal annual soil loss risk mapping employing Revised Universal Soil Loss Equation (RUSLE) model in Nun Nadi Watershed, Uttrakhand (India). Arab J Geosci 6(10):4045–4056. https://doi.org/10.1007/s12517-012-0661-z

Nehaï SA, Guettouche MS (2020) Soil loss estimation using the revised universal soil loss equation and a GIS-based model: a case study of Jijel Wilaya, Algeria. Arab J Geosci 13:152. https://doi.org/10.1007/s12517-020-5160-z

Nyesheja EM, Chen X, El-Tantawi AM, Karamage F, Mupenzi C, Nsengiyumva JB (2019) Soil erosion assessment using RUSLE model in the Congo Nile Ridge region of Rwanda. Phys Geogr 40(4):339–360. https://doi.org/10.1080/02723646.2018.1541706

Ouabid M, Ouali H, Garrido CJ, Acosta-Vigil A, Román-Alpiste MJ, Dautria JM, Marchesi C, Hidas K (2017) Neoproterozoic granitoids in the basement of the Moroccan Central Meseta: correlation with the Anti-Atlas at the NW paleo-margin of Gondwana. Precambrian Res 299:34–57. https://doi.org/10.1016/j.precamres.2017.07.007

Ouassou A, Amziane TH, Lajouad L (2006) State of natural resources degradation in Morocco and plan of action for desertification and drought control, in: Desertification in the Mediterranean Region. A Security Issue. Springer, pp 251–268. https://doi.org/10.1007/1-4020-3760-0_10

Pal SC, Chakrabortty R (2019) Modeling of water induced surface soil erosion and the potential risk zone prediction in a sub-tropical watershed of Eastern India. Model Earth Syst Environ 5(2):369–393. https://doi.org/10.1007/s40808-018-0540-z

Phinzi K, Ngetar NS (2019) The assessment of water-borne erosion at catchment level using GIS-based RUSLE and remote sensing: a review. Int Soil Water Conserv Res 7(1):27–46. https://doi.org/10.1016/j.iswcr.2018.12.002

Pimentel D, Burgess M (2013) Soil erosion threatens food production. Agriculture 3(3):443–463

Pradeep GS, Krishnan MVN, Vijith H (2015) Identification of critical soil erosion prone areas and annual average soil loss in an upland agricultural watershed of Western Ghats, using analytical hierarchy process (AHP) and RUSLE techniques. Arab J Geosci 8(6):3697–3711. https://doi.org/10.1007/s12517-014-1460-5

Prasannakumar V, Vijith H, Abinod S, Geetha N (2012) Estimation of soil erosion risk within a small mountainous sub-watershed in Kerala, India, using Revised Universal Soil Loss Equation (RUSLE) and geo-information technology. Geosci Front 3(2):209–215. https://doi.org/10.1016/j.gsf.2011.11.003

Rahman MR, Shi ZH, Chongfa C (2009) Soil erosion hazard evaluation—an integrated use of remote sensing, GIS and statistical approaches with biophysical parameters towards management strategies. Ecol Model 220(13-14):1724–1734. https://doi.org/10.1016/j.ecolmodel.2009.04.004

Rango A, Arnoldus HMJ (1987) Aménagement des bassins versants. Cahiers techniques de la FAO, pp 1–11

Renard KG (1997) Predicting soil erosion by water: a guide to conservation planning with the revised universal soil loss equation (RUSLE), Agriculture handbook. USDA, Washington, D. C.

Renard KG, Foster GR, Weesies GA, Porter JP (1991) RUSLE: revised universal soil loss equation. J Soil Water Conserv 46(1):30–33

Rey F, Ballais JL, Marre A, Rovéra G (2004) Rôle de la végétation dans la protection contre l'érosion hydrique de surface. CR Geosci 336(11):991–998. https://doi.org/10.1016/j.crte.2004.03.012

Roose E (1994) Introduction à la gestion conservatoire de l'eau, de la biomasse et de la fertilité des sols. FAO - Soil Bull 70:85-87

Roy RN, Misra RV, Lesschen JP, Smaling EM (2005) Evaluation du bilan en elements nutritifs du sol. Approches et methodologies. Food and Agriculture Organization, Rome

Sadiki A, Bouhlassa S, Auajjar J, Faleh A, Macaire JJ (2004) Utilisation d'un SIG pour l'évaluation et la cartographie des risques d'érosion par l'Equation universelle des pertes en sol dans le Rif oriental (Maroc): cas du bassin versant de l'oued Boussouab. Bull Inst Sci, Rabat, Sect Sci Terre 26:69–79

Saha A, Ghosh M, Pal SC (2020) Understanding the morphology and development of a rill-gully: an empirical study of Khoai Badland, West Bengal, India. In: Shit PK, Pourghasemi HR, Bhunia GS (eds) Gully Erosion Studies from India and Surrounding Regions, Advances in Science. Technology & Innovation. Springer International Publishing, Cham, pp 147–161. https://doi.org/10.1007/978-3-030-23243-6_9

Sharpley AN, Williams JR (1990) EPIC-erosion/productivity impact calculator: 1. Model documentation. US Department of Agriculture, Agricultural Research Service

Shrimali SS, Aggarwal SP, Samra JS (2001) Prioritizing erosion-prone areas in hills using remote sensing and GIS — a case study of the Sukhna Lake catchment, Northern India. Int J Appl Earth Obs Geoinf 3(1):54–60. https://doi.org/10.1016/S0303-2434(01)85021-2

Smith HJ (1999) Application of empirical soil loss models in southern Africa: a review. S Afr J Plant Soil 16(3): 158–163. https://doi.org/10.1080/02571862.1999.10635003

Snoussi M (1988) Nature, estimation et comparaison des flux de matieres issus des bassins versants de l'Adour (France), du Sebou, de l'Oum-er-Rbia et du Souss (Maroc): impact du climat sur les apports fluviatiles a l'ocean. PhD Thesis, Bordeaux University

Sun W, Shao Q, Liu J, Zhai J (2014) Assessing the effects of land use and topography on soil erosion on the Loess Plateau in China. Catena 121:151–163. https://doi.org/10.1016/j.catena.2014.05.009

Taib Y, Touil A, Aissa M, Hibti M, Zouhair M, Ouadjou A (2020) Geochemistry and petrogenesis of early Ediacaran volcanic rocks from taourirte district (Western High Atlas, Morocco): origin and geodynamic implications. J Afr Earth Sci 170:103936. https://doi.org/10.1016/j.jafrearsci.2020.103936

Tairi A, Elmouden A, Aboulouafa M (2019) Soil erosion risk mapping using the analytical hierarchy process (AHP) and geographic information system in the Tifnout-Askaoun watershed, Southern Morocco. Eur Sci J 15:338–338

Teng H, Liang Z, Chen S, Liu Y, Rossel RAV, Chappell A, Yu W, Shi Z (2018) Current and future assessments of soil erosion by water on the Tibetan Plateau based on RUSLE and CMIP5 climate models. Sci Total Environ 635:673–686. https://doi.org/10.1016/j.scitotenv.2018.04.146

Tian YC, Zhou YM, Wu BF, Zhou WF (2009) Risk assessment of water soil erosion in upper basin of Miyun Reservoir, Beijing, China. Environ Geol 57:937–942. https://doi.org/10.1007/s00254-008-1376-z

Tuo D, Xu M, Gao G (2018) Relative contributions of wind and water erosion to total soil loss and its effect on soil properties in sloping croplands of the Chinese Loess Plateau. Sci Total Environ 633: 1032–1040. https://doi.org/10.1016/j.scitotenv.2018.03.237

Uddin K, Murthy MSR, Wahid SM, Matin MA (2016) Estimation of soil erosion dynamics in the Koshi basin using GIS and remote sensing to assess priority areas for conservation. PLoS One 11(3):e0150494. https://doi.org/10.1371/journal.pone.0150494

USDA (1951) Soil survey manual (USDA Handbook 18)

Vaezi AR, Zarrinabadi E, Auerswald K (2017) Interaction of land use, slope gradient and rain sequence on runoff and soil loss from weakly aggregated semi-arid soils. Soil Tillage Res 172:22–31. https://doi.org/10.1016/j.still.2017.05.001

Van Pelt RS, Hushmurodov SX, Baumhardt RL, Chappell A, Nearing MA, Polyakov VO, Strack JE (2017) The reduction of partitioned wind and water erosion by conservation agriculture. Catena 148(2): 160–167. https://doi.org/10.1016/j.catena.2016.07.004

Wachal DJ, Hudak PF (2000) Mapping landslide susceptibility in Travis County, Texas, USA. GeoJournal 51(3):245–253. https://doi.org/10.1023/A:1017524604463

Williams JR, Singh VP (1995) Computer models of watershed hydrology. In: Singh VP (ed) The EPIC Model. Water Resources Publications, Highlands Ranch, CO, pp 909–1000

Wischmeier WH, Smith DD (1978) Predicting rainfall erosion losses-a guide to conservation planning. In: Predicting Rainfall Erosion Losses-A Guide to Conservation Planning. USDA, Science and Education Administration, Hyattsville

Xu L, Xu X, Meng X (2013) Risk assessment of soil erosion in different rainfall scenarios by RUSLE model coupled with Information Diffusion Model: a case study of Bohai Rim, China. Catena 100: 74–82. https://doi.org/10.1016/j.catena.2012.08.012

Zhang L, Bai KZ, Wang MJ, Karthikeyan R (2016) Basin-scale spatial soil erosion variability: Pingshuo opencast mine site in Shanxi Province, Loess Plateau of China. Nat Hazards 80(2):1213–1230. https://doi.org/10.1007/s11069-015-2019-9